2018

A Study of Epithelial Cl- Secretion in the Murine Distal Colon

Trey S Rottgen

A Study of Epithelial Cl^- Secretion in the Murine Distal Colon

Trey S. Rottgen

Dissertation submitted

to the School of Medicine at West Virginia University
in partial fulfillment of the requirements for the degree of
Doctor of Philosophy in Cellular and Integrative Physiology

David Siderovski, Ph.D., Chair

Stanley Hileman, Ph.D.

HanGang Yu, Ph.D.

Justin Kupec, M.D.
Vazhaikkurichi Rajendran, Ph.D.

Department of Physiology, Pharmacology, and Neuroscience

Morgantown, West Virginia 2018

Keywords: KCNQ, TMEM16A, Ussing chamber, Colon, DSS, ENS

ABSTRACT

A Study of Epithelial Cl^- Secretion in the Murine Distal Colon

Trey S. Rottgen

Colonic epithelium has an on-going basal level of Cl^- secretion, which is necessary for maintaining a properly hydrated epithelial mucus layer, and the movement of waste products. However, alterations in the level of Cl^- secretion can have significant effects. Loss of colonic Cl^- secretion, such as that seen in Cystic Fibrosis or ulcerative colitis can result in intestinal obstruction. While infection with *Vibrio cholera* or increased activity of the Enteric nervous system (ENS) can result in increased Cl^- secretion and resultant diarrhea. In this study, we decided to evaluate both sides of the spectrum via an animal model of inflammatory bowel disease, and study ENS regulation of epithelial Cl^- secretion.

Ulcerative colitis (UC) is well-characterized to have a significant attenuation in colonic Cl^- secretion. An animal model of UC, which utilizes the epithelial irritant dextran-sulfate sodium (DSS), has also been shown to have significantly blunted epithelial Cl^- secretion. More specifically, previous observations have demonstrated the loss of Ca^{2+}-activated Cl^- secretion. Therefore in our study, we examined Ca^{2+}-activated Cl^- secretion in murine distal colon mounted in Ussing chamber. A subset of animals underwent a chronic induction model of DSS-colitis. Animals that received DSS demonstrated a loss of Ca^{2+}-activated Cl^- secretion when stimulated with carbochol in Ussing chamber experiments. Protein isolated from colonic epithelium of DSS-colitis animals demonstrated a significant decrease in the Ca^{2+}-activated Cl^- channel, TMEM16A. This would indicate that loss of TMEM16A in colonic epithelium following DSS-treatment contributes to the observed loss of Ca^{2+}-activated Cl^- secretion in functional studies.

ENS activity has previously been observed to contribute to the measured Cl^- secretion in colonic epithelium. Therefore, we decided to evaluate the efficacy of KCNQ K^+ channel activators to hyperpolarize and decrease enteric neuronal signaling. Flupirtine, a pan-KCNQ activator, was able to significantly inhibit on-going Cl^- secretion measured as a function of short-circuit current (I_{SC}) in Ussing chamber preparations. Application of tetrodotoxin (TTX), following flupirtine, was unable to inhibit Cl^- secretion, however reversal of order of application resulted in a significant inhibition of Cl^- secretion via TTX. Immunofluorescence studies also demonstrated the co-localization of KCNQ2 and KCNQ3 with axons of enteric neurons positively-labeled with choline acetyltransferase. From these results, we conclude that activation of KCNQ2 and KCNQ3 in enteric neurons is able to inhibit basal Cl^- secretion in colonic epithelium.

ACKNOWLEDGEMENTS

First of all, I would like to thank my Wife, Melissa, for all of her support, especially in recent months leading up to this point. She not only makes wonderful food, but also has been a great help going through this process due to her own experiences. I would not be here without her assistance. So, I just want to say thank you so very much for your love and support. And of course being the greatest dog mom Cooper could ever ask for.

I would to thank my family for always being there for me. I especially want to thank my Mom for the tremendous job she did in raising me, and giving me basically all the tools to succeed. She's the hardest working person I know and always has this calm and collected manner even when things are difficult. I know I am not as good as she is but staying calm under pressure is one of my defining attributes, and I completely contribute that to my Mom. Also, a thanks to my brother for always putting up with me (even though I was annoying). High school and College were so easy because of your tips you always gave to me.

I would like to thank Dr. Greg Dick and Drew Fancher for really opening the door to research. I am forever grateful to them for taking the time to mentor some silly little undergraduate that had way too many questions.

I also would like to thank my labmates, Drew and Emily, for putting up with me the past couple of years. It has been a ton of fun, and I will truly miss working with and seeing you guys on a regular basis.

Of course, I need to thank Dr. Rajendran (Raj) for allowing me to join his lab. Working for him I have learned a tremendous amount about India and more

importantly how to “get things in black”. I would like to thank my committee members: Drs. Stanley Hileman, David Siderovski, Justin Kupec, and HanGang Yu for their helpful advice and professional mentorship.

Thank you, Everyone.

ABBREVIATIONS

NHE3	Sodium/Hydrogen Exchanger 3
DRA	Down-regulated in Adenoma
ENaC	Epithelial Sodium Channel
CFTR	Cystic Fibrosis Transmembrane Regulator
FSK	Forskolin
CaCC	Ca^{2+}-activated Cl^- Channel
FRET	Fluorescence Resonance Energy Transfer
HEK	Human Embryonic Kidney
EC_{50}	Half-maximal Excitatory Concentration
ENS	Enteric Nervous System
CNS	Central Nervous System
IPAN	Intrinsic Primary Afferent Neuron
Na_V	Voltage-sensitive Sodium Channel
TTX	Tetrodotoxin
ACh	Acetylcholine
KCNQ	Voltage-sensitive K^+ channel
cRNA	Complementary RNA
TEA	Tetraethylammonium
GI	Gastrointestinal
IBD	Inflammatory Bowel Disease
UC	Ulcerative Colitis
DSS	Dextran-Sulfate Sodium

siRNA	Small Interfering RNA
CCH	Carbochol
TMEM16A	Ca^{2+}-activated Cl^- Channel
ITPR3	IP_3 Receptor
I_{SC}	Short-Circuit Current
Flu	Flupirtine
TOL	Tolterodine
ICA	ICA-110381
NICO	Nicotine
XE-991	KCNQ Antagonist
IC_{50}	Half-maximal Inhibitory Concetration

Chapter I

INTRODUCTION

The function of the large intestine (colon) is primarily to absorb water from the lumen, participate in electrolyte homeostasis, and propel waste forward for elimination in the form of feces.

For the average adult, the colon absorbs approximately 1.5-2 liters of water each day [1]. This can increase to as much as 5-6 liters of water absorption in the circumstance of increased volume presentation [2]. However, volumes exceeding this limit or presentation of a large bulk volume will result in diarrhea. Water absorption is heavily reliant on electrolyte transport in the colon, as evidenced by several pathologies that lead to excess luminal electrolytes and resultant water loss [3]. However, the relative contribution of the paracellular versus transcellular pathways is still under investigation [4].

Electrolyte transport within the colon is accomplished via movement through a paracellular and transcellular pathway [1]. Paracellular movement makes up the largest component, however as contents progress distally within the colon, the transcellular component increases [1]. The paracellular component is simply movement of electrolytes down a concentration gradient, but the transcellular movement is performed via a myriad of transporters and ion channels that line the colonic mucosa. Together, the two pathways are able to absorb approximately 100 mmol/L of Na^+ each day, with an astounding upper limit of 400 mmol/L per day [5].

Elimination of waste following water and electrolyte absorption is driven by a complex series of coordinated muscle contractions that propel the feces forward for elimination via defecation. The muscle contractions are not under

conscious control or even under the control of the central nervous system for the most part. This is primarily accomplished by a nervous system of the gastrointestinal tract known as the enteric nervous system [6].

These separate, but incredibly intermingled tasks are accomplished via an interaction between the absorptive surface or epithelium of the colonic mucosa and the enteric nervous system. The following chapter will provide greater detail on both the epithelial layer and enteric nervous system, as well as elaborate on an ion channels specific to each.

Colonic Epithelium

The epithelial layer lining the colonic lumen consists of a simple columnar epithelium intermixed with mucus-secreting goblet cells [7]. The organization of epithelium at the level of the cell consists of an apical membrane that is exposed to luminal contents, and a basolateral membrane that interacts directly with the interstitial space. This kind of organization gives the epithelial cells a type of “polarity” upon differentiation that is simply the localization of different transporters [7]. Epithelial cells are anchored to a basement membrane and other epithelial cells via tight junction proteins [8]. The purpose of a “tight” epithelial layer is to minimize interaction between the “outside” and the host’s immune system [9]. Histological examination of the colonic epithelium reveals a repeating pattern of crypts of Lieberkuhn followed by surface cells [7]. The historical paradigm characterizes these different locations as secretory cells located within the crypts and absorptive cells localized at the surface of the mucosa [10, 11].

Whether this is actually the case is debatable, however this provides an avenue to discuss some general electrolyte transport within the colon.

The primary cation that is absorbed in the colon is the monovalent Na^+ ion [12]. In the proximal portions and to a lesser degree in distal portions of the colon, Na^+ is absorbed via the electroneutral transporter sodium/hydrogen exchanger isoform 3 (NHE3) [13]. NHE3 is coupled to the down-regulated in adenoma (DRA) transporter that exchanges Cl^- and HCO_3^- [14, 15]. This mechanism is coupled via pH changes within the cellular microenvironment that absorbs a single Na^+ coupled with absorption of a single Cl^-, while extruding a proton and single HCO_3^- molecule [14]. Upon moving to a more distal location within the colon, Na^+ absorption changes from handling via NHE3 to the electrogenic, epithelial Na^+ channel (ENaC) [16, 17]. The movement of Na^+ through ENaC is mediated by a favorable electrochemical gradient that is generated via Na^+/K^+ atpase, which is located on the basolateral membrane [7]. The "pump" moves intracellular Na^+ to the interstitial space and creates a void by which extracellular Na^+ located on the apical side of the membrane can move down its electrochemical gradient [18]. Also, the movement of Na^+ into the cell and eventual basolateral extrusion via the Na^+/K^+ pump causes absorption of water (H_2O) via paracellular movement or aquaporin proteins located within apical membranes of colonic epithelium [19, 20].

While Na^+ absorption is a major component of on-going electrolyte transport within the colon, the presence of an electrogenic anion secretion is present [21]. In Ussing chamber studies, the majority of observed short-circuit

current (I_{SC}) can be attributed to apical anion secretion. The primary component of this basal anion secretion is comprised of the Cystic Fibrosis transmembrane regulator (CFTR) [22, 23]. The channel is so named due to its association with the disease Cystic Fibrosis. It was characterized to mediate the observed pathology in the early 1990s [24, 25]. The channel is a cAMP-sensitive Cl^- channel that has a single-channel conductance of only 8-12 pS [26, 27]. However, stimulation with basolateral forskolin (FSK) can induce observable currrents in either whole-cell patch clamp electrophysiology or Ussing chamber. At the time of identification of the CFTR channel or lack thereof in CF patients, many researchers observed the presence of a compensatory Cl^- current [28, 29]. This additional Cl^- current seemed to be activated more through Ca^{2+}-sensitive pathways instead of intracellular production of cyclic nucleotides [28-30].

The Ca^{2+}-activated Cl^- channel (CaCC) was initially observed in *Xenopus oocytes* [31]. The channel demonstrated a slight voltage and time-dependence upon activation at lower Ca^{2+} concentrations. Also, the channel was sensitive to inhibition by niflumic acid with an apparent K_i of 17 μM [31]. Several potential CaCCs have been proposed; however practically all putative candidates did not demonstrate a similar electrophysiological profile to the CaCC initially described in *Xenopus oocytes* [32-34]. More recently though, three separate groups identified a CaCC that resembles the native current in electrophysiological terms [35-37]. Since the identification of this new putative CaCC, it has been named TMEM16A. The initial studies on TMEM16A demonstrated the channel to be localized to salivary and cultured human bronchial epithelial cells [35, 36].

Following these initial observations, another group utilizing a global knock-out mouse of TMEM16A demonstrated an absence of a Ca^{2+}-activated Cl^- current in mouse trachea [38].

Similar to the reports of TMEM16A-mediating the Ca^{2+}-activated Cl^- current in native respiratory epithelium, the mice were also used to study colonic epithelium [38, 39]. Transepithelial potential [V_{TE}] of distal colon administered basolateral carbachol (CCH; cholinergic agonist that increases intracellular Ca^{2+} concentration) was able to significantly hyperpolarize in *Tmem16a*$^{+/+}$ mice [38]. However, *Tmem16a*$^{-/-}$ littermates were not able to respond to basolateral CCH administration [38]. Calculated I_{SC} from control animals was approximately 60 μA/cm^2, while *Tmem16a*$^{-/-}$ animals had a calculated I_{SC} of about 10 μA/cm^2 [38]. It was not until recently that the tissue-specific [*Vil1*] knock-out mice of TMEM16A confirmed the previously observed results [40]. Similar to the global knockout mice, CCH-stimulated I_{SC} was significantly less in the *Tmem16a*$^{-/-}$ animals [40].

TMEM16A has been observed in several human colonic epithelial cell lines. The HT-29 and T_{84} cell lines have both demonstrated expression of TMEM16A, characterized by immunoblot [41, 42]. However, a group that employed the use of siRNA targeted against TMEM16A in the T_{84} cell line did not demonstrate a large decrease in ATP-stimulated I_{SC} [43]. The only change in the measured I_{SC} was the initial peak prior to the plateau phase of the trace, which would potentially indicate a minor role for TMEM16A in human colonic epithelium [43]. However, ATP-stimulated I_{SC} in T_{84} cells has previously been characterized to be

mediated more through adenosine receptors, instead of Ca^{2+}-increasing purinergic receptors [44].

Characterization of the Ca^{2+}-activated Cl^- Channel TMEM16A

Considerable research has also focused on the physical characterization of TMEM16A [45-47]. One of the initial findings suggested that the final quaternary structure of TMEM16A existed as a dimer in the plasma membrane [48]. This was demonstrated with TMEM16A proteins that were fused to either GFP or mCherry [48]. The different TMEM16A conjugates were able to undergo fluorescence resonance energy transfer [FRET], which indicated a close proximity of the two proteins [48]. However, it was not until a couple of years later that the actual sequence of amino acids important for this interaction was identified [49]. Mutants of TMEM16A lacking an α-helix that corresponded to residues 161-179 were not able to form functional channels, hence the lack of observed Cl^- currents in transfected HEK 293 cells [49].

Shortly after this discovery, a group was able to identify several residues that were important for the voltage-dependence of the channel, as well as amino acids that participate in the Ca^{2+}-sensitivity of TMEM16A [50]. The residues that confer a voltage-dependence of the channel were found to be located within the first intracellular loop and consisted of four repeating glutamic acid residues [$_{444}$EEEE] [Fig. 1] [50]. Alanine substitution at these residues shifted the half-maximal activation of the channel from 64 ± 0.9 mV to a more depolarized potential of ≈160 mV at 1 μM Ca^{2+} [50]. Also, the residues important for Ca^{2+}-

sensitivity were found to be located directly adjacent to the glutamic acid residues and consisted of a glutamic acid, alanine, valine, and lysine [$_{448}$EAVK] [Fig. 1] [50]. Deletion of these particular residues was able to shift the Ca^{2+}-sensitivity drastically from 1 μM (which was able to increase open-probability at very hyperpolarized potentials) to 25 μM Ca^{2+} (which could increase open-probability only marginally) [50]. While EAVK residues are undoubtedly important for channel gating, it has also been shown that glutamic acid residues [E702/705] are also essential for Ca^{2+}-sensitivity of TMEM16A [Fig. 1] [51]. This was demonstrated by mutants of these two residues having a Ca^{2+}-sensitivity several orders of magnitude less than their respective wild-type [WT] channel [[Ca^{2+}], 20 μM WT vs. 2 mM E702/705 M] [51]. The importance of these residues was confirmed by another group that mutated these same amino acids and obtained a channel with significantly less Ca^{2+}-sensitivity [52]. This group was able to demonstrate cooperativity between these residues and the amino acids initially found to confer sensitivity [$_{448}$EAVK] [52]. Three other acidic moieties [E650, E730, D734] have been shown to contribute to the Ca^{2+}-sensitivity of TMEM16A [51]. Also, Scudieri et al. developed TMEM16A chimera proteins by substituting residues from TMEM16B [another member of the protein family, also exhibiting Ca^{2+}-stimulated Cl^- secretion] into the sequence of TMEM16A to determine potential domains necessary for Ca^{2+}-binding [53]. The group was able to determine from their results that the third intracellular loop of TMEM16A participates in conferring Ca^{2+}-sensitivity to the channel [53]. This was made

obvious by the deletion of these residues resulting in a shift of the EC_{50} of Ca^{2+} from 0.25 μM to 2 μM at a holding potential of +100 mV [53].

While the previously mentioned work was essential for identifying residues necessary for Ca^{2+}-binding and voltage-sensitivity [50, 51, 53], it was not until the crystal structure was elucidated that researchers could more clearly visualize the interaction of the previously mentioned residues [and several others] in Ca^{2+}-binding and channel gating of TMEM16A [54]. In 2014, Brunner et al. were the first group to generate a crystal structure of TMEM16 from *Nectria haematococca* [nhTMEM16] [54]. The conserved protein from *Nectria haematococca* only functions as a lipid scramblase, however, the protein is still sensitive to Ca^{2+} and demonstrates increased scramblase activity with increasing concentrations of Ca^{2+} [54]. The results of the study were able to demonstrate that nhTMEM16 does in fact associate as a dimer in the plasma membrane [54]. This study also described a Ca^{2+}-binding segment that was embedded within the hydrophobic membrane [54]. This research group was also the first one to postulate the possible mechanisms of ion conductance by either a single pore or double-barreled architecture [46, 54]. Following the initial observations obtained from the crystal structure of nhTMEM16, two different groups were able to resolve the crystal structure of TMEM16A from murine origin [47, 55, 56]. This new information about the channel was able to illuminate important residues for interaction with conducting anions as well as illustrate that each monomer of TMEM16A was able to bind two individual Ca^{2+} ions [55]. Also, the greater resolution with the murine TMEM16A allowed for an accurate description of how

Ca^{2+}-binding mediates Cl^- conductance [56]. This is accomplished via a hinge mechanism that is dependent on a glutamic acid residue [E654] interacting with two Ca^{2+} ions that allow for opening of a single pore within the channel [56].

As evidenced by the tremendous amount of research that has been conducted on the characterization of TMEM16A there is still much to be done in the future. Hopefully, the previous observations can be utilized to further characterize the channel in regard to potential protein-protein interactions, or the development of novel antagonists that allow for the pharmacological study of the channel in isolation. Also, some preliminary evidence indicates a potential role for the channel in several pathologies. Whatever the case, research will continue on the CaCC, TMEM16A.

Enteric Nervous System

The enteric nervous system (ENS) in humans contains about as many neurons as the entire spinal cord, which is approximately 500 million neurons [57]. Due to the ENS containing so many neurons, it has previously been referred to as the "mini-brain of the gut". Almost every neurotransmitter that has been identified in the central nervous system (CNS) has also been observed in the ENS [58]. The complexity of the ENS is so vast that the majority of the gastrointestinal tract can function with local control from ENS neurons, instead of extrinsic signals from the CNS [59, 60]. The ENS has the ability to regulate local blood flow in the tissue, motility of the tract, and electrolyte secretion via control of epithelial tissue [61]. The ENS is primarily localized to two major layers: the submucosal plexus and the myenteric plexus [6]. The submucosal plexus is

located just beneath the submucosa, while the myenteric plexus is actually located between the two smooth muscle layers of the GI tract (circular and longitudinal).

Whether located within the myenteric or submucosal plexus, there is a wide variety of neurons that contribute to the proper functioning of the gastrointestinal tract, however, they can be generally subdivided into afferent and efferent limbs of the ENS. Intrinsic primary afferent neurons (IPANs) have axons that sample the luminal contents for noxious stimuli that could cause harm to the mucosal layer, as well as, exhibiting an ability to respond to inflammatory mediators [62-64]. Integration of these signals can lead to a reflexive arc utilizing other ENS neurons or the stimulation of a centrally-mediated arc to increase motility and secretion to dilute and eliminate any potential hazard [61]. While the IPANs are sensory in function, the ENS is not without effector neurons such as secretomotor neurons [6]. Axons originating from the secretomotor neurons can stretch either in an ascending or descending longitudinal fashion as to coordinate an overall complex response of rhythmic muscle contractions [6, 65]. Some of these axons may even project to the mucosa to synapse on epithelium [66]. With this type of patterned distribution, the secretomotor neurons are able to increase/decrease contraction of the smooth muscle of the GI tract and in turn increase or decrease motility, as well as, signal to the epithelial layer to modify on-going electrolyte transport depending on the current synaptic inputs [6, 66].

As far as signaling within the ENS, many different neurotransmitters are utilized regardless of whether the neuron is a secretomotor neuron or IPAN [58].

However, cholinergic fibers (acetylcholine-releasing, ACh) comprise approximately 60% of the total fibers within the ENS [67]. In many cases, ACh is released along with small neuropeptides such as vasoactive intestinal peptide or calcitonin-gene related peptide, which contribute to the overall observed response [58]. ACh that is released from secretomotor neurons mediates its effect through muscarinic receptors located on smooth muscle or the basolateral surface of the epithelium. The binding of ACh to a muscarinic receptor leads to a transient increase in intracellular Ca^{2+}, which may mediate a contraction of smooth muscle or an increase in Cl^- secretion from epithelium, depending on the localization of release [68, 69].

While the released neurotransmitter is the actual molecule that can modulate the activity of its target, it is universally understood that ion channels located on a neuron can regulate the release of said neurotransmitter [70, 71]. Previous studies have shown that blockade of voltage-sensitive Na^+ channels (Na_V) with tetrodotoxin (TTX) can prevent release of neurotransmitter via inhibition of the propagating action potentials [72]. Neurotransmitter release can also be inhibited in this same fashion from enteric neurons [73, 74]. However, the generation of an action potential and eventual release of a neurotransmitter is dependent on the cell reaching a threshold potential.

Hyperpolarization via activation of K^+ channels in neurons can prevent synaptic inputs from reaching a threshold potential. More specifically though, activation of KCNQ (K_V7) channels or the “M” current in CNS neurons is able to cause a significant hyperpolarization and inhibition of neurotransmitter release

[75]. A previous group has also shown that activation of K_V7 channels on neuronal cell membranes of the ENS can cause a dramatic hyperpolarization and prevent IPANs from responding to the noxious stimulus bradykinin [76]. The group was also able to show that distension with supraphysiological pressures was unable to generate an action potential when neurons were hyperpolarized via activation of KCNQ channels.

Characterization of KCNQ Channels

KCNQ channels are voltage-sensitive K^+ channels (K_V) [77, 78]. All members of the family consist of six transmembrane domains [79, 80]. The fourth of which is the S4 domain and confers the voltage-sensitivity to the KCNQ family, as well as, all voltage-sensitive K^+ channels [81-83]. The group is composed of five different isoforms, which are simply KCNQ1-KCNQ5 [77, 84-86]. Similar to many other K^+ channels [87-89], the KCNQ family associates in the membrane as a tetramer to form the functional channel [90, 91]. These channels have been characterized as slowly deactivating with visible currents at hyperpolarized potentials [92]. The family of channels are also frequently referred to as the “M” current. This is due to early observations that stimulating the M_1 receptor would inhibit the visible current [93, 94]. However, stimulation of receptors for angiotensin II, bradykinin, or purines will cause inhibition of the current or really any other Gαq activation pathway [95-97]. The KCNQ family has also been characterized as contributing to resting membrane potential in many different cell types [98-101]. The channels have been functionally identified and have been shown to play a major role in a vast array of tissues, including vestibular hair

cells of the inner ear, cortical neurons, cardiac repolarization, and K^+ recycling in respiratory and colonic epithelium [102-106]. Several pathologies, which include a form of deafness, a familial type of epilepsy, as well as the long QT syndrome in the heart have been linked to mutations in one variant or another [102, 107, 108]. The aforementioned diseases also demonstrate the functional importance of KCNQ channels in cellular membranes.

While several different isoforms of the KCNQ family exist, only a couple have real functional significance in neuronal tissue. KCNQ2 ($K_V7.2$) and KCNQ3 ($K_V7.3$) are the primary contributors to the M current in neuronal tissue, however, in some peripheral circuits KCNQ5 ($K_V7.5$) has been identified [101, 109, 110]. Early observations of the neuronal M current demonstrated that the current, as previously mentioned, could be inhibited via activation of muscarinic receptors [94]. The mechanism of inhibition would later be shown to be PIP_2 depletion in the cellular membrane [111]. It was also shown that the native M current could dampen the excitability of neurons and therefore reduce the amount of action potentials [112, 113].

In 1998, Biervert et al. was able to clone the open-reading frame of one of these channels, KCNQ2 [114]. The study was able to show that not only was this in fact a voltage-sensitive K^+ channel, but mutations in the channel were directly linked to a neonatal seizure disorder through the cloning of a mutant isoform from a patient [114]. In that same year, Wang et al. was able to not only clone KCNQ2 independently, but also clone KCNQ3 [77]. In vitro transcribed cRNA of KCNQ2 and KCNQ3 was injected into *Xenopus oocytes* and voltage-clamped for

functional characterization [77]. KCNQ2, as previously described, had observable currents, however, injection of KCNQ3 alone did not produce currents above that of background [77]. Co-expression of the two isoforms increased the observed currents dramatically. Also, the co-expression of the two channels seemed to affect sensitivity to the inhibitor tetraethylammonium (TEA), since the previous K_d for KCNQ2 alone was much less than during co-expression of both channels (0.16 ± 0.02 mM vs. 3.5 ± 0.7 mM) [77]. More importantly though, the study was able to show that co-expression of the two channels resulted in a profile that was similar to the native M current in half-activation (-45.4 mV vs. -46.7 mV, M vs. KCNQ2/3) and pharmacological inhibition to XE-991 (0.98 ± 0.15 μM vs. 0.6 ± 0.1 μM, M vs. KCNQ2/3) [77]. This was a major discovery in identifying the putative neuronal M current channels.

Animal models utilizing genetic manipulations have been very useful in determining the importance of KCNQ2 and KCNQ3 in neuronal physiology. In 2005, a group utilized a dominant-negative knock-in of KCNQ2 [112]. M currents were significantly less than wild-type littermates. Also, spike-frequency was significantly increased in neurons expressing the KCNQ2 dominant-negative. Unfortunately, a genetic deletion model of KCNQ2 resulted in death of peri-natal mice within only a few hours of birth [115]. Less has been done with KCNQ3, however, one group did develop a model utilizing a substitution of glycine to valine at position 311 [116]. This specific mutation is derived from a family that was well characterized to have benign familial neonatal convulsions. Animals homozygous for this mutation demonstrated a significant attrition rate as

compared to heterozygotes. Elicited current upon a step protocol demonstrated a significantly blunted response to depolarizing potentials.

Following some of these observations that clearly indicated KCNQ2/3 were important to overall neuronal excitability, it was shown that the channels associated with ankyrin-G in axon initial segments (AIS) [117, 118]. This interaction was shown to be mediated via several c-terminal residues. Substitution of those residues in KCNQ2 (E810A, S811A, D812A) and KCNQ3 (E837A, T838A, D839A) (Fig. 2) resulted in loss of localization to the AIS in cultured hippocampal neurons [118]. Shah et al. developed a small peptide that was able to disrupt this interaction in brain slices undergoing patch clamp electrophysiology [119]. Application of the ankyrin-binding-peptide (ABP) did result in an overall depolarization of hippocampal neurons. More interestingly though, the disruption in the AIS led to a dramatic reduction (7.8 ± 0.8 mV) in the threshold potential for generation of an action potential [119].

Another residue that may have less importance for channel localization but definitely has significance in terms of modulation of channel activity is the residue important for binding of several pharmaceuticals such as retigabine and flupirtine. Both have been shown to be potent activators of native M current, as well as expressed KCNQ2 and KCNQ2/3 subunits [120, 121]. The substitution of a single tryptophan (W236 Q2/ W265 Q3) (Fig. 2) can result in complete loss of sensitivity to retigabine [122, 123]. The proposed mechanism is that binding to the tryptophan can stabilize the activation gate, which would increase activation, as well as, slow deactivation of the channel (Both phenomenon have been

observed in electrophysiology experiments) [123]. Flupirtine has not been scrutinized in this same way. However, the drug shares substantial homology to retigabine and is assumed to promote channel activation in a similar manner.

Inflammatory bowel Disease

This group of diseases are characterized as inflammation along the gastrointestinal tract (GI), primarily occurring in the distal portions of the small intestine and all throughout the colon [124]. Inflammatory bowel disease (IBD) is primarily two different diseases, which are Crohn's disease and ulcerative colitis. Crohn's disease while normally localized to the small and large bowel can potentially manifest in any portion of the GI tract. Also, Crohn's disease can elicit inflammation throughout the entire thickness of the bowel, ranging from the epithelial layer to the underlying longitudinal smooth muscle [125]. This can result in the formation of strictures or even bowel perforations. However, ulcerative colitis (UC) is only localized to the large bowel. It is clinically characterized as inflammation beginning within the rectum and moving proximally. In severe cases of pancolitis (inflammation of the entire colon), "inflammatory backwash" can move into the distal ileum of the small bowel causing inflammation. As far as inflammation within the tissue, UC is typically isolated to the mucosa (epithelium) and submucosa [126]. Besides differences in the location of the two diseases, the two pathologies also have a different profile when it comes to the inflammatory response. Crohn's Disease typically has a cytokine profile that resembles a Th_1 response, while UC is more typically a Th_2 response [125, 126]. While this information has provided avenues for the development of new

therapies, the actual etiology of either disease is still unknown and under intense research.

Since tissue from a patient can only be obtained upon manifestation of the disease, many animal models have been utilized to more fully understand the pathogenesis of IBD [127]. One of the more common models utilized for IBD research is the dextran-sulfate sodium (DSS)-induced colitis model [128-130]. The model has been shown to have consistent results as well as offering ease of replication. Animals that undergo DSS exposure are simply administered their normal drinking water supplemented with 2-5% DSS [128]. The size of the dextran has been shown to impact the severity of colitis that develops within animal. The typical size that is utilized within the literature is 36,000-50,000 daltons [131, 132]. The overall histopathological features that develop are similar to IBD with a large inflammatory infiltrate in the laminia propria, crypt distortion, and crypt abscesses [133]. However, selection of the host has been shown to impact the elicited inflammatory response. C57Bl/6 mice when exposed to DSS typically develop Th_1-type response (Crohn's disease), but Balb/c mice when administered DSS develop more of a Th_2 inflammatory response, which is more similar to the clinical pathology of UC [126, 134, 135].

Specific Aims:

Specific Aim 1: To determine if the observed absence of Ca^{2+}-activated Cl^- secretion in DSS-colitis is the result of the down-regulation of the Ca^{2+}-activated Cl^- channel, TMEM16A. To evaluate this, functional evidence will be collected utilizing the Ussing chamber to measure epithelial Cl^- secretion from mounted colonic epithelium from either control or DSS-colitis mice. Also, protein expression/localization of TMEM16A will also be evaluated using immunoblot and immunohistochemistry techniques.

Specific Aim 2: To determine if activation of KCNQ channels in enteric neurons can inhibit apical Cl^- secretion via hyperpolarization and resultant inhibition of neurotransmitter release. Mounted colonic epithelium from murine distal colon will have flupirtine (KCNQ activator) applied to the basolateral membrane in the presence or absence of other inhibitors of the ENS. Also, co-localization via immunofluorescence of KCNQ2 and KCNQ3 with choline acetyl transferase will be carried out to determine the presence of and potential contributors to the observed effect in functional studies.

References

1. Sandle, G.I., *Salt and water absorption in the human colon: a modern appraisal.* Gut, 1998. **43**(2): p. 294-9.
2. Debongnie, J.C. and S.F. Phillips, *Capacity of the human colon to absorb fluid.* Gastroenterology, 1978. **74**(4): p. 698-703.
3. Ghishan, F.K. and P.R. Kiela, *Epithelial transport in inflammatory bowel diseases.* Inflamm Bowel Dis, 2014. **20**(6): p. 1099-109.
4. Spring, K.R., *Routes and mechanism of fluid transport by epithelia.* Annu Rev Physiol, 1998. **60**: p. 105-19.
5. Shields, R. and J.B. Miles, *Absorption and Secretion in the Large Intestine.* Postgrad Med J, 1965. **41**: p. 435-9.
6. Costa, M., S.J. Brookes, and G.W. Hennig, *Anatomy and physiology of the enteric nervous system.* Gut, 2000. **47 Suppl 4**: p. iv15-9; discussion iv26.
7. Geibel, J.P., *Secretion and absorption by colonic crypts.* Annu Rev Physiol, 2005. **67**: p. 471-90.
8. Lee, S.H., *Intestinal permeability regulation by tight junction: implication on inflammatory bowel diseases.* Intest Res, 2015. **13**(1): p. 11-8.
9. Piche, T., *Tight junctions and IBS--the link between epithelial permeability, low-grade inflammation, and symptom generation?* Neurogastroenterol Motil, 2014. **26**(3): p. 296-302.
10. Bohme, M., M. Diener, and W. Rummel, *Calcium- and cyclic-AMP-mediated secretory responses in isolated colonic crypts.* Pflugers Arch, 1991. **419**(2): p. 144-51.

11. Welsh, M.J., et al., *Crypts are the site of intestinal fluid and electrolyte secretion.* Science, 1982. **218**(4578): p. 1219-21.

12. Giller, J. and S.F. Phillips, *Electrolyte absorption and secretion in the human colon.* Am J Dig Dis, 1972. **17**(11): p. 1003-11.

13. Schultheis, P.J., et al., *Renal and intestinal absorptive defects in mice lacking the NHE3 Na+/H+ exchanger.* Nat Genet, 1998. **19**(3): p. 282-5.

14. Melvin, J.E., et al., *Mouse down-regulated in adenoma (DRA) is an intestinal Cl(-)/HCO(3)(-) exchanger and is up-regulated in colon of mice lacking the NHE3 Na(+)/H(+) exchanger.* J Biol Chem, 1999. **274**(32): p. 22855-61.

15. Moseley, R.H., et al., *Downregulated in adenoma gene encodes a chloride transporter defective in congenital chloride diarrhea.* Am J Physiol, 1999. **276**(1 Pt 1): p. G185-92.

16. Malsure, S., et al., *Colon-specific deletion of epithelial sodium channel causes sodium loss and aldosterone resistance.* J Am Soc Nephrol, 2014. **25**(7): p. 1453-64.

17. Duc, C., et al., *Cell-specific expression of epithelial sodium channel alpha, beta, and gamma subunits in aldosterone-responsive epithelia from the rat: localization by in situ hybridization and immunocytochemistry.* J Cell Biol, 1994. **127**(6 Pt 2): p. 1907-21.

18. Silva, P., A.N. Charney, and F.H. Epstein, *Potassium adaptation and Na-K-ATPase activity in mucosa of colon.* Am J Physiol, 1975. **229**(6): p. 1576-9.

19. Bleakman, D. and R.J. Naftalin, *Hypertonic fluid absorption from rabbit descending colon in vitro.* Am J Physiol, 1990. **258**(3 Pt 1): p. G377-90.

20. Levitan, R., et al., *Water and salt absorption in the human colon.* J Clin Invest, 1962. **41**: p. 1754-9.

21. Frizzell, R.A. and J.W. Hanrahan, *Physiology of epithelial chloride and fluid secretion.* Cold Spring Harb Perspect Med, 2012. **2**(6): p. a009563.

22. Zhou, L., et al., *Correction of lethal intestinal defect in a mouse model of cystic fibrosis by human CFTR.* Science, 1994. **266**(5191): p. 1705-8.

23. Cozens, A.L., et al., *CFTR expression and chloride secretion in polarized immortal human bronchial epithelial cells.* Am J Respir Cell Mol Biol, 1994. **10**(1): p. 38-47.

24. Kartner, N., et al., *Expression of the cystic fibrosis gene in non-epithelial invertebrate cells produces a regulated anion conductance.* Cell, 1991. **64**(4): p. 681-91.

25. Dalemans, W., et al., *Altered chloride ion channel kinetics associated with the delta F508 cystic fibrosis mutation.* Nature, 1991. **354**(6354): p. 526-8.

26. Schwiebert, E.M., et al., *CFTR regulates outwardly rectifying chloride channels through an autocrine mechanism involving ATP.* Cell, 1995. **81**(7): p. 1063-73.

27. Bear, C.E., et al., *Purification and functional reconstitution of the cystic fibrosis transmembrane conductance regulator (CFTR).* Cell, 1992. **68**(4): p. 809-18.

28. Schoumacher, R.A., et al., *A cystic fibrosis pancreatic adenocarcinoma cell line.* Proc Natl Acad Sci U S A, 1990. **87**(10): p. 4012-6.

29. Knowles, M.R., L.L. Clarke, and R.C. Boucher, *Activation by extracellular nucleotides of chloride secretion in the airway epithelia of patients with cystic fibrosis.* N Engl J Med, 1991. **325**(8): p. 533-8.

30. Wagner, J.A., et al., *Activation of chloride channels in normal and cystic fibrosis airway epithelial cells by multifunctional calcium/calmodulin-dependent protein kinase.* Nature, 1991. **349**(6312): p. 793-6.

31. Takahashi, T., E. Neher, and B. Sakmann, *Rat brain serotonin receptors in Xenopus oocytes are coupled by intracellular calcium to endogenous channels.* Proc Natl Acad Sci U S A, 1987. **84**(14): p. 5063-7.

32. Gandhi, R., et al., *Molecular and functional characterization of a calcium-sensitive chloride channel from mouse lung.* J Biol Chem, 1998. **273**(48): p. 32096-101.

33. Gruber, A.D., et al., *Genomic cloning, molecular characterization, and functional analysis of human CLCA1, the first human member of the family of Ca2+-activated Cl- channel proteins.* Genomics, 1998. **54**(2): p. 200-14.

34. Cunningham, S.A., et al., *Cloning of an epithelial chloride channel from bovine trachea.* J Biol Chem, 1995. **270**(52): p. 31016-26.

35. Yang, Y.D., et al., *TMEM16A confers receptor-activated calcium-dependent chloride conductance.* Nature, 2008. **455**(7217): p. 1210-5.

36. Caputo, A., et al., *TMEM16A, a membrane protein associated with calcium-dependent chloride channel activity.* Science, 2008. **322**(5901): p. 590-4.

37. Schroeder, B.C., et al., *Expression cloning of TMEM16A as a calcium-activated chloride channel subunit.* Cell, 2008. **134**(6): p. 1019-29.

38. Ousingsawat, J., et al., *Loss of TMEM16A causes a defect in epithelial Ca2+-dependent chloride transport.* J Biol Chem, 2009. **284**(42): p. 28698-703.

39. Rock, J.R., et al., *Transmembrane protein 16A (TMEM16A) is a Ca2+-regulated Cl- secretory channel in mouse airways.* J Biol Chem, 2009. **284**(22): p. 14875-80.

40. Benedetto, R., et al., *Epithelial Chloride Transport by CFTR Requires TMEM16A.* Sci Rep, 2017. **7**(1): p. 12397.

41. Sun, H., et al., *Tgf-beta downregulation of distinct chloride channels in cystic fibrosis-affected epithelia.* PLoS One, 2014. **9**(9): p. e106842.

42. Tian, Y., et al., *Control of TMEM16A by INO-4995 and other inositolphosphates.* Br J Pharmacol, 2013. **168**(1): p. 253-65.

43. Namkung, W., P.W. Phuan, and A.S. Verkman, *TMEM16A inhibitors reveal TMEM16A as a minor component of calcium-activated chloride channel conductance in airway and intestinal epithelial cells.* J Biol Chem, 2011. **286**(3): p. 2365-74.

44. Stutts, M.J., et al., *Activation of CFTR Cl- conductance in polarized T84 cells by luminal extracellular ATP.* Am J Physiol, 1995. **268**(2 Pt 1): p. C425-33.

45. Jeng, G., et al., *Independent activation of distinct pores in dimeric TMEM16A channels.* J Gen Physiol, 2016. **148**(5): p. 393-404.

46. Lim, N.K., A.K. Lam, and R. Dutzler, *Independent activation of ion conduction pores in the double-barreled calcium-activated chloride channel TMEM16A.* J Gen Physiol, 2016. **148**(5): p. 375-392.

47. Paulino, C., et al., *Structural basis for anion conduction in the calcium-activated chloride channel TMEM16A.* Elife, 2017. **6**.

48. Sheridan, J.T., et al., *Characterization of the oligomeric structure of the Ca(2+)-activated Cl- channel Ano1/TMEM16A.* J Biol Chem, 2011. **286**(2): p. 1381-8.

49. Tien, J., et al., *Identification of a dimerization domain in the TMEM16A calcium-activated chloride channel (CaCC).* Proc Natl Acad Sci U S A, 2013. **110**(16): p. 6352-7.

50. Xiao, Q., et al., *Voltage- and calcium-dependent gating of TMEM16A/Ano1 chloride channels are physically coupled by the first intracellular loop.* Proc Natl Acad Sci U S A, 2011. **108**(21): p. 8891-6.

51. Tien, J., et al., *A comprehensive search for calcium binding sites critical for TMEM16A calcium-activated chloride channel activity.* Elife, 2014. **3**.

52. Han, Y., et al., *Two Ca(2+)-Binding Sites Cooperatively Couple Together in TMEM16A Channel.* J Membr Biol, 2016. **249**(1-2): p. 57-63.

53. Scudieri, P., et al., *Intermolecular Interactions in the TMEM16A Dimer Controlling Channel Activity.* Sci Rep, 2016. **6**: p. 38788.

54. Brunner, J.D., et al., *X-ray structure of a calcium-activated TMEM16 lipid scramblase.* Nature, 2014. **516**(7530): p. 207-12.

55. Dang, S., et al., *Cryo-EM structures of the TMEM16A calcium-activated chloride channel.* Nature, 2017. **552**(7685): p. 426-429.

56. Paulino, C., et al., *Activation mechanism of the calcium-activated chloride channel TMEM16A revealed by cryo-EM.* Nature, 2017. **552**(7685): p. 421-425.

57. Furness, J.B., *Types of neurons in the enteric nervous system.* J Auton Nerv Syst, 2000. **81**(1-3): p. 87-96.

58. Furness, J.B., et al., *Intrinsic primary afferent neurons and nerve circuits within the intestine.* Prog Neurobiol, 2004. **72**(2): p. 143-64.

59. Thomas, J.a.K.A., *A Study of Gastro-Intestinal Motility in Relation to the Enteric Nervous System.* American Journal of Physiology, 1926: p. 606-626.

60. Bayliss, W.M. and E.H. Starling, *The movements and innervation of the small intestine.* J Physiol, 1899. **24**(2): p. 99-143.

61. Furness, J.B., et al., *The enteric nervous system and gastrointestinal innervation: integrated local and central control.* Adv Exp Med Biol, 2014. **817**: p. 39-71.

62. Bertrand, P.P., et al., *Analysis of the responses of myenteric neurons in the small intestine to chemical stimulation of the mucosa.* Am J Physiol, 1997. **273**(2 Pt 1): p. G422-35.

63. Gao, C., et al., *Serine proteases excite myenteric neurons through protease-activated receptors in guinea pig small intestine.* Gastroenterology, 2002. **123**(5): p. 1554-64.

64. Frieling, T., et al., *Neuroimmune communication in the submucous plexus of guinea pig colon after infection with Trichinella spiralis.* Gastroenterology, 1994. **107**(6): p. 1602-9.

65. Furness, J.B., et al., *Intrinsic primary afferent neurons of the intestine.* Prog Neurobiol, 1998. **54**(1): p. 1-18.

66. Jones, S.L. and A.T. Blikslager, *Role of the enteric nervous system in the pathophysiology of secretory diarrhea.* J Vet Intern Med, 2002. **16**(3): p. 222-8.

67. Qu, Z.D., et al., *Immunohistochemical analysis of neuron types in the mouse small intestine.* Cell Tissue Res, 2008. **334**(2): p. 147-61.

68. Mitsui, M. and H. Karaki, *Dual effects of carbachol on cytosolic Ca2+ and contraction in intestinal smooth muscle.* Am J Physiol, 1990. **258**(5 Pt 1): p. C787-93.

69. Mall, M., et al., *Cholinergic ion secretion in human colon requires coactivation by cAMP.* Am J Physiol, 1998. **275**(6 Pt 1): p. G1274-81.

70. Hemmings, H.C., Jr., *Sodium channels and the synaptic mechanisms of inhaled anaesthetics.* Br J Anaesth, 2009. **103**(1): p. 61-9.

71. Lipscombe, D., S. Kongsamut, and R.W. Tsien, *Alpha-adrenergic inhibition of sympathetic neurotransmitter release mediated by modulation of N-type calcium-channel gating.* Nature, 1989. **340**(6235): p. 639-42.

72. Kostyuk, P.G., N.S. Veselovsky, and A.Y. Tsyndrenko, *Ionic currents in the somatic membrane of rat dorsal root ganglion neurons-I. Sodium currents.* Neuroscience, 1981. **6**(12): p. 2423-30.

73. Chandan, R., et al., *Cholinergic neurons and muscarinic receptors regulate anion secretion in pig distal jejunum.* Eur J Pharmacol, 1991. **193**(3): p. 265-73.

74. Belai, A., J. Lincoln, and G. Burnstock, *Lack of release of vasoactive intestinal polypeptide and calcitonin gene-related peptide during electrical stimulation of enteric nerves in streptozotocin-diabetic rats.* Gastroenterology, 1987. **93**(5): p. 1034-40.

75. Hernandez, C.C., et al., *Regulation of neural KCNQ channels: signalling pathways, structural motifs and functional implications.* J Physiol, 2008. **586**(7): p. 1811-21.

76. Peiris, M., et al., *Peripheral KV7 channels regulate visceral sensory function in mouse and human colon.* Mol Pain, 2017. **13**: p. 1744806917709371.

77. Wang, H.S., et al., *KCNQ2 and KCNQ3 potassium channel subunits: molecular correlates of the M-channel.* Science, 1998. **282**(5395): p. 1890-3.

78. Schroeder, B.C., et al., *A constitutively open potassium channel formed by KCNQ1 and KCNE3.* Nature, 2000. **403**(6766): p. 196-9.

79. Robbins, J., *KCNQ potassium channels: physiology, pathophysiology, and pharmacology.* Pharmacol Ther, 2001. **90**(1): p. 1-19.

80. Choveau, F.S. and M.S. Shapiro, *Regions of KCNQ K(+) channels controlling functional expression.* Front Physiol, 2012. **3**: p. 397.

81. Long, S.B., E.B. Campbell, and R. Mackinnon, *Voltage sensor of Kv1.2: structural basis of electromechanical coupling.* Science, 2005. **309**(5736): p. 903-8.

82. Jiang, Y., et al., *X-ray structure of a voltage-dependent K+ channel.* Nature, 2003. **423**(6935): p. 33-41.

83. Jiang, Y., et al., *The principle of gating charge movement in a voltage-dependent K+ channel.* Nature, 2003. **423**(6935): p. 42-8.

84. Lerche, C., et al., *Molecular cloning and functional expression of KCNQ5, a potassium channel subunit that may contribute to neuronal M-current diversity.* J Biol Chem, 2000. **275**(29): p. 22395-400.

85. Kubisch, C., et al., *KCNQ4, a novel potassium channel expressed in sensory outer hair cells, is mutated in dominant deafness.* Cell, 1999. **96**(3): p. 437-46.

86. Yang, W.P., et al., *KvLQT1, a voltage-gated potassium channel responsible for human cardiac arrhythmias.* Proc Natl Acad Sci U S A, 1997. **94**(8): p. 4017-21.

87. Jiang, Y., et al., *Crystal structure and mechanism of a calcium-gated potassium channel.* Nature, 2002. **417**(6888): p. 515-22.

88. MacKinnon, R., *Determination of the subunit stoichiometry of a voltage-activated potassium channel.* Nature, 1991. **350**(6315): p. 232-5.

89. Doyle, D.A., et al., *The structure of the potassium channel: molecular basis of K+ conduction and selectivity.* Science, 1998. **280**(5360): p. 69-77.

90. Smith, J.A., et al., *Structural models for the KCNQ1 voltage-gated potassium channel.* Biochemistry, 2007. **46**(49): p. 14141-52.

91. Nakajo, K., et al., *Stoichiometry of the KCNQ1 - KCNE1 ion channel complex.* Proc Natl Acad Sci U S A, 2010. **107**(44): p. 18862-7.

92. Jentsch, T.J., *Neuronal KCNQ potassium channels: physiology and role in disease.* Nat Rev Neurosci, 2000. **1**(1): p. 21-30.

93. Marrion, N.V., et al., *Muscarinic suppression of the M-current in the rat sympathetic ganglion is mediated by receptors of the M1-subtype.* Br J Pharmacol, 1989. **98**(2): p. 557-73.

94. Brown, D.A. and P.R. Adams, *Muscarinic suppression of a novel voltage-sensitive K+ current in a vertebrate neurone.* Nature, 1980. **283**(5748): p. 673-6.

95. Adams, P.R., D.A. Brown, and A. Constanti, *Pharmacological inhibition of the M-current.* J Physiol, 1982. **332**: p. 223-62.

96. Shapiro, M.S., L.P. Wollmuth, and B. Hille, *Angiotensin II inhibits calcium and M current channels in rat sympathetic neurons via G proteins.* Neuron, 1994. **12**(6): p. 1319-29.

97. Cruzblanca, H., D.S. Koh, and B. Hille, *Bradykinin inhibits M current via phospholipase C and Ca2+ release from IP3-sensitive Ca2+ stores in rat sympathetic neurons.* Proc Natl Acad Sci U S A, 1998. **95**(12): p. 7151-6.

98. Yeung, S.Y. and I.A. Greenwood, *Electrophysiological and functional effects of the KCNQ channel blocker XE991 on murine portal vein smooth muscle cells.* Br J Pharmacol, 2005. **146**(4): p. 585-95.

99. Evseev, A.I., et al., *Functional effects of KCNQ K(+) channels in airway smooth muscle.* Front Physiol, 2013. **4**: p. 277.

100. Anderson, U.A., C. Carson, and K.D. McCloskey, *KCNQ currents and their contribution to resting membrane potential and the excitability of interstitial cells of Cajal from the guinea pig bladder.* J Urol, 2009. **182**(1): p. 330-6.

101. Wladyka, C.L. and D.L. Kunze, *KCNQ/M-currents contribute to the resting membrane potential in rat visceral sensory neurons.* J Physiol, 2006. **575**(Pt 1): p. 175-89.

102. Ackerman, M.J., et al., *A novel mutation in KVLQT1 is the molecular basis of inherited long QT syndrome in a near-drowning patient's family.* Pediatr Res, 1998. **44**(2): p. 148-53.

103. MacVinish, L.J., et al., *Xe991 reveals differences in K(+) channels regulating chloride secretion in murine airway and colonic epithelium.* Mol Pharmacol, 2001. **60**(4): p. 753-60.

104. Moser, S.L., et al., *Multiple KCNQ potassium channel subtypes mediate basal anion secretion from the human airway epithelial cell line Calu-3.* J Membr Biol, 2008. **221**(3): p. 153-63.

105. Cooper, E.C., et al., *M channel KCNQ2 subunits are localized to key sites for control of neuronal network oscillations and synchronization in mouse brain.* J Neurosci, 2001. **21**(24): p. 9529-40.

106. Rennie, K.J., T. Weng, and M.J. Correia, *Effects of KCNQ channel blockers on K(+) currents in vestibular hair cells.* Am J Physiol Cell Physiol, 2001. **280**(3): p. C473-80.

107. Schwake, M., et al., *Surface expression and single channel properties of KCNQ2/KCNQ3, M-type K+ channels involved in epilepsy.* J Biol Chem, 2000. **275**(18): p. 13343-8.

108. Leitner, M.G., et al., *Restoration of ion channel function in deafness-causing KCNQ4 mutants by synthetic channel openers.* Br J Pharmacol, 2012. **165**(7): p. 2244-59.

109. Shah, M., et al., *Molecular correlates of the M-current in cultured rat hippocampal neurons.* J Physiol, 2002. **544**(Pt 1): p. 29-37.

110. Otto, J.F., et al., *A spontaneous mutation involving Kcnq2 (Kv7.2) reduces M-current density and spike frequency adaptation in mouse CA1 neurons.* J Neurosci, 2006. **26**(7): p. 2053-9.

111. Zhang, H., et al., *PIP(2) activates KCNQ channels, and its hydrolysis underlies receptor-mediated inhibition of M currents.* Neuron, 2003. **37**(6): p. 963-75.

112. Peters, H.C., et al., *Conditional transgenic suppression of M channels in mouse brain reveals functions in neuronal excitability, resonance and behavior.* Nat Neurosci, 2005. **8**(1): p. 51-60.

113. Santini, E. and J.T. Porter, *M-type potassium channels modulate the intrinsic excitability of infralimbic neurons and regulate fear expression and extinction.* J Neurosci, 2010. **30**(37): p. 12379-86.

114. Biervert, C., et al., *A potassium channel mutation in neonatal human epilepsy.* Science, 1998. **279**(5349): p. 403-6.

115. Watanabe, H., et al., *Disruption of the epilepsy KCNQ2 gene results in neural hyperexcitability.* J Neurochem, 2000. **75**(1): p. 28-33.

116. Singh, N.A., et al., *Mouse models of human KCNQ2 and KCNQ3 mutations for benign familial neonatal convulsions show seizures and neuronal plasticity without synaptic reorganization.* J Physiol, 2008. **586**(14): p. 3405-23.

117. Inda, M.C., J. DeFelipe, and A. Munoz, *Voltage-gated ion channels in the axon initial segment of human cortical pyramidal cells and their relationship with chandelier cells.* Proc Natl Acad Sci U S A, 2006. **103**(8): p. 2920-5.

118. Rasmussen, H.B., et al., *Requirement of subunit co-assembly and ankyrin-G for M-channel localization at the axon initial segment.* J Cell Sci, 2007. **120**(Pt 6): p. 953-63.

119. Shah, M.M., et al., *Functional significance of axonal Kv7 channels in hippocampal pyramidal neurons.* Proc Natl Acad Sci U S A, 2008. **105**(22): p. 7869-74.

120. Klinger, F., et al., *Concomitant facilitation of GABAA receptors and KV7 channels by the non-opioid analgesic flupirtine.* Br J Pharmacol, 2012. **166**(5): p. 1631-42.

121. Tatulian, L. and D.A. Brown, *Effect of the KCNQ potassium channel opener retigabine on single KCNQ2/3 channels expressed in CHO cells.* J Physiol, 2003. **549**(Pt 1): p. 57-63.

122. Kim, R.Y., et al., *Atomic basis for therapeutic activation of neuronal potassium channels.* Nat Commun, 2015. **6**: p. 8116.

123. Schenzer, A., et al., *Molecular determinants of KCNQ (Kv7) K+ channel sensitivity to the anticonvulsant retigabine.* J Neurosci, 2005. **25**(20): p. 5051-60.

124. Abraham, C. and J.H. Cho, *Inflammatory bowel disease.* N Engl J Med, 2009. **361**(21): p. 2066-78.

125. Gajendran, M., et al., *A comprehensive review and update on Crohn's disease.* Dis Mon, 2018. **64**(2): p. 20-57.

126. Danese, S. and C. Fiocchi, *Ulcerative colitis.* N Engl J Med, 2011. **365**(18): p. 1713-25.

127. Goyal, N., et al., *Animal models of inflammatory bowel disease: a review.* Inflammopharmacology, 2014. **22**(4): p. 219-33.

128. Chassaing, B., et al., *Dextran sulfate sodium (DSS)-induced colitis in mice.* Curr Protoc Immunol, 2014. **104**: p. Unit 15 25.

129. Rottgen, T.S., et al., *Dextran Sulfate Sodium (DSS)-induced Chronic Colitis Attenuates Ca(2+)-activated Cl(-) Secretion in Murine Colon by Down-regulating TMEM16A.* Am J Physiol Cell Physiol, 2018.

130. Okayasu, I., et al., *A novel method in the induction of reliable experimental acute and chronic ulcerative colitis in mice.* Gastroenterology, 1990. **98**(3): p. 694-702.

131. Kitajima, S., S. Takuma, and M. Morimoto, *Histological analysis of murine colitis induced by dextran sulfate sodium of different molecular weights.* Exp Anim, 2000. **49**(1): p. 9-15.

132. Hirono, I., et al., *Carcinogenicity of dextran sulfate sodium in relation to its molecular weight.* Cancer Lett, 1983. **18**(1): p. 29-34.

133. Cooper, H.S., et al., *Clinicopathologic study of dextran sulfate sodium experimental murine colitis.* Lab Invest, 1993. **69**(2): p. 238-49.

134. Mahler, M., et al., *Differential susceptibility of inbred mouse strains to dextran sulfate sodium-induced colitis.* Am J Physiol, 1998. **274**(3 Pt 1): p. G544-51.

135. Dieleman, L.A., et al., *Chronic experimental colitis induced by dextran sulphate sodium (DSS) is characterized by Th1 and Th2 cytokines.* Clin Exp Immunol, 1998. **114**(3): p. 385-91.

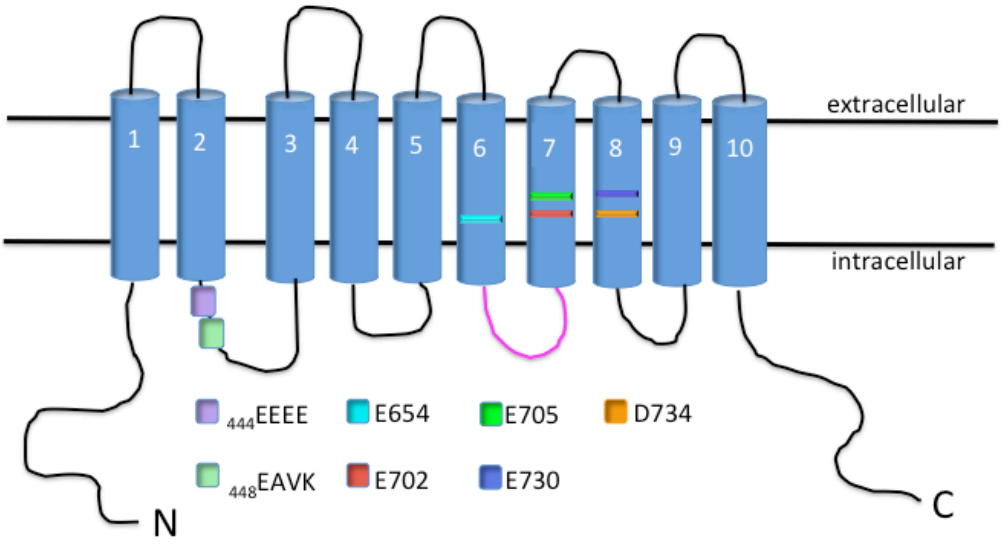

Figure 1. Schematic of TMEM16A channel protein with identified residues necessary for voltage and Ca^{2+}-sensitivity. TMEM16A channel protein consists of 10 transmembrane domains [TMD]. The intracellular loop between TMD-2 and TMD-3 contains the voltage-sensitive $_{444}$EEEE residues, as well as, the $_{448}$EAVK residues that participate in Ca^{2+}-sensitivity of the channel. The E702 and E705 residues located within the seventh TMD also participate in Ca^{2+}-sensitivity of the channel. The third intracellular loop (shown in pink), and the residues E654, E730 and D734 have also been implicated to affect Ca^{2+}-sensitivity of the channel.

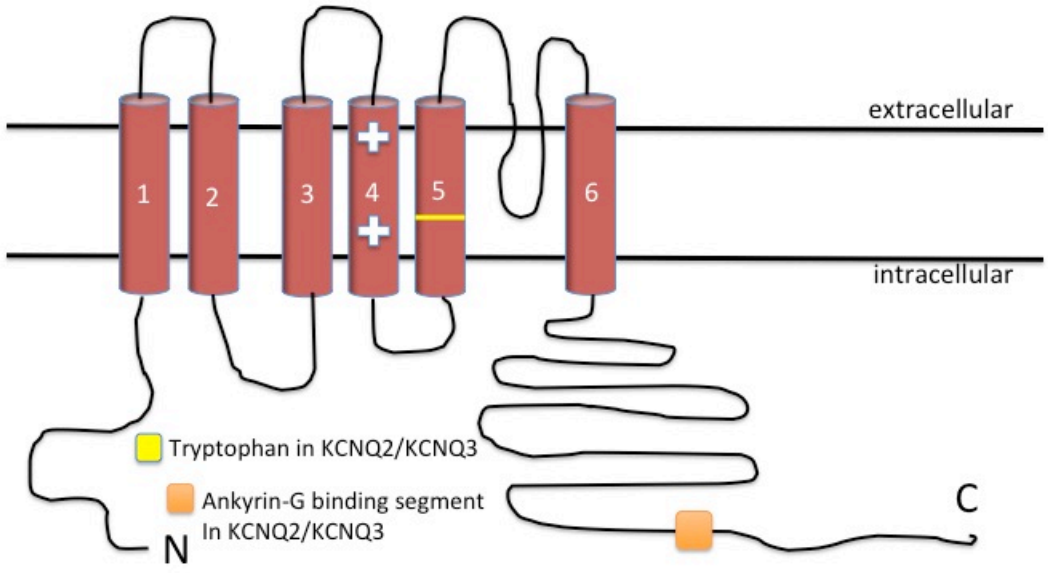

Figure 2. Schematic of KCNQ2 and KCNQ3 channels with labeled residues important for drug binding and channel localization. Tryptophan (W 236 Q2/ W 265 Q3) labeled in yellow is necessary for binding of retigabine and the homologous drug, flupirtine. The orange box correlates to residues important for localization to axon initial segments (AIS). Deletion or substitution of these residues results in a complete loss of localization. The S4 domain is important voltage-sensitivity of the channel (hence labeling with the positive signs).

Chapter II

Dextran Sulfate Sodium (DSS)-induced Chronic Colitis Attenuates Ca^{2+}-activated Cl^- Secretion in Murine Colon by Down-regulating TMEM16A

Trey S. Rottgen[1,2], Andrew J. Nickerson[1,2], Emily A. Minor[1,2], Amanda B. Stewart[3], Abby D. Harold[1,2] and Vazhaikkurichi M. Rajendran[1,2]

[1]Department of Physiology, Pharmacology, and Neuroscience, West Virginia University School of Medicine, Morgantown, West Virginia
[2]Department of Biochemistry and Molecular Pharmacology, West Virginia University School of Medicine, Morgantown, West Virginia
[3]Department of Biology, Bethany College, Bethany, West Virginia

Running Title: Decreased TMEM16A Expression in DSS-induced Colitis

Key Words: Ussing Chamber, Colonic epithelium, Cl^- channels, Muscarinic Signaling, Colitis,

Abstract. Attenuated Ca^{2+}-activated Cl^- secretion has previously been observed in the model of dextran-sulfate-sodium (DSS)-induced colitis. Prior studies have implicated dysfunctional muscarinic signaling from basolateral membranes as the potential perpetrator leading to decreased Ca^{2+}-activated Cl^- secretion. However, in our chronic model of DSS-colitis, *Chrm3* transcript (1.028 ± 0.12 vs. 1.029 ± 0.27, $p > 0.05$) and CHRM3 protein expression (1.021 ± .24 vs. .928 ± .09, $p > 0.05$) were unchanged. Therefore, we hypothesized that decreased CCH-stimulated Cl^- secretion in DSS-induced colitis can be attributed to a loss of Ca^{2+}-activated Cl^- channels (CaCC) in apical membranes of colonic epithelium. To establish chemically-induced colitis, Balb/C mice were exposed to 4% DSS for 5 alternating weeks to stimulate a more moderate, chronic colitis. Upon completion of the protocol, whole thickness sections of colon were mounted in the Ussing chamber under voltage-clamp conditions. DSS-induced colitis demonstrated a complete inhibition of basolateral administration of CCH-stimulated Cl^- secretion that actually displayed a reversal in polarity (15.40 ± 2.22 $\mu A/cm^2$ vs. -2.47±0.25 $\mu A/cm^2$). Western blot of potential CaCCs, quantified by densitometric analysis, demonstrated no change in bestrophin-2 (BEST2) and cystic fibrosis transmembrane regulator (CFTR), while Anoctamin-1 (ANO1, TMEM16A) was significantly down-regulated (1.001 ± 0.13 vs. 0.510 ± 0.12, $p < 0.05$). Our findings indicate that decreased expression of TMEM16A in DSS-induced colitis contributes to the decreased Ca^{2+}-activated Cl^- secretion in murine colon.

Introduction

Chloride secretion in secretory epithelium has been primarily subdivided into cAMP-stimulated and Ca^{2+}-activated through the use of different pharmacological agonists (9, 13). Aberrations in Cl^- secretion have been observed in several pathological conditions, which include Cystic Fibrosis, Vibrio cholera infection, and inflammatory bowel disease (8, 14, 37). Decreased Cl^- secretion in ulcerative colitis (UC) or animal models of UC (dextran-sulfate sodium; DSS) has been previously reported (10, 12). More specifically, Ca^{2+}-activated Cl^- secretion has been shown to be decreased in the DSS-induced colitis animal model (3, 16, 19). Previous studies focused on this phenomenon concluded the attenuation to be attributable to dysfunctional muscarinic signaling from the basolateral surface of colonic epithelium (1, 18). However more recently, it has been reported to be possible perturbations in ion channel function/expression in colonic epithelium (16).

Ca^{2+}-activated Cl^- channels (CaCCs) have been implicated to be involved in epithelial differentiation, salivary secretion and mucociliary clearance (28, 30, 35). However initial attempts to characterize CaCCs proved difficult, as potential candidates did not match the biophysical properties of the native protein (15). In the past decade a novel CaCC, anoctamin 1 (ANO1, TMEM16A), was identified by three separate groups (6, 34, 40). Young et al demonstrated that injected siRNA to *Tmem16a* significantly inhibited pilocarpine (muscarinic agonist)-stimulated salivary secretion in mice (40), while Caputo et al was able to achieve a similar knockdown of Ca^{2+}-activated Cl^- secretion with siRNA targeted to

TMEM16A in primary human bronchial epithelial cells (6). Following these seminal discoveries, several groups utilizing a global gene knock-out of *Tmem16a* demonstrated the absence of Ca^{2+}-activated Cl^- secretion in secretory epithelium isolated from trachea and colon (28, 30). However, the global deletion of the gene resulted in tracheal malacia and premature death of the animal (29). More recently, a tissue-specific knock-out of *Tmem16a* was developed. Isolated distal colon from these mice demonstrated an absence of Ca^{2+}-activated Cl^- secretion following CCH administration (4).

While TMEM16A has been identified as the primary mediator of Ca^{2+}-activated Cl^- secretion in colonic epithelium, it has not been studied in DSS-induced colitis. Thus, the goal of this study was to identify as to whether the previously described decreased Ca^{2+}-activated Cl^- secretion in colonic epithelium was attributable to decreased expression of TMEM16A in a DSS-induced chronic colitis. Our results indicate that TMEM16A protein expression is down-regulated in a chronic model of DSS-induced colitis and contributes to the observed loss in Ca^{2+}-activated Cl^- secretion.

Materials and Methods

Animals. Non-fasting male Balb/cAnNCrl mice (17 weeks old, Charles River, NY) were provided normal chow for the entirety of the project. Prior to the beginning of the 10-week project, mice (7 weeks) were randomly selected for either control or DSS groups, respectively. Balb/C mice selected for the DSS protocol were provided 4% DSS for 5 days (with 9 days of normal drinking water in between) for 5 alternating weeks, beginning with the first week. Animals utilized for the acute protocol were assigned to either control or DSS groups. DSS groups were administered 4.5% DSS in the drinking water for five (5) consecutive days followed by one day of normal drinking water. Both groups were then euthanized on the seventh day of the protocol. All animals used in the study were provided food and water ad libitum. All animals were anesthetized with intraperitoneal (*i.p.)* injection of Fatal Plus (Patterson Veterinary, SC). The experimental protocols used in this study were approved by the West Virginia University Institutional Animal Care and Use Committee.

Histology and Immunohistochemistry. Distal colon segments were isolated from euthanized mice via bilateral pneumothorax. Isolated colonic segments were measured immediately upon removal with a constant temperature of 22-23^{o}C. Distal colon segments were then rinsed with phosphate-buffered saline (PBS) to remove any residual content and debris. Colonic segments were then opened longitudinally along the mesenteric border. An approximate 3 mm piece of segment was then cut from the intact colon and immediately placed in 10% neutral-buffered formalin for tissue fixation. Fixed tissue was then given to the

West Virginia University Translational Pathology Department for paraffin-embedding and haemotoxylin and eosin (H&E) staining. Prepared slides consisted of 5 μm thick sections mounted on glass slides, followed by H&E staining for visualization of tissue architecture from the respective treatment groups. Immunohistochemistry was also performed on control and DSS tissue by the West Virginia University Translational Pathology Department to determine the localization of TMEM16A in whole thickness sections of mouse distal colon. Anti-TMEM16A antibody (Alomone, Jerusalem, Israel) was used at a dilution of 1:100. Sectioned tissue was incubated at 37^{o}C for a period of one hour in primary antibody. Following the initial step, tissue was incubated in goat anti-rabbit horseradish-peroxidase conjugated secondary antibody (1:1000) for one hour. Finally, a chromogenic substrate was added for visualization of immune-stained slides. All images were captured with the AxioImager (Carl Zeiss, Germany) on a 20x magnification.

Electrophysiology. Distal Colons were removed from euthanized mice via bilateral pneumothorax and rinsed with ice-cold PBS to clear residual contents. Segments were opened longitudinally along the mesenteric border to expose the epithelium. Full thickness tissue was then mounted on a pin slider with an oval aperture of 2.8 w x 11 l mm with a cross-sectional area of 0.30 cm^2 and placed in the EasyMount Ussing chamber (Physiological Instruments, San Diego, CA) for electrophysiological study as previously described (26). Mounted tissue was bathed on both sides with Ringers' solution (in mM: 115 NaCl, 25 $NaHCO_3$, 2.4 K_2HPO_4, 0.4 KH_2PO_4, 1.2 $CaCl_2$, 1.2 $MgCl_2$ and 10 glucose), while also being

continuously voltage-clamped at 0 mV to abolish any developing electrochemical gradient. I_{SC} was continuously monitored with a 5 mV pulse applied to the tissue every 5 s to measure resistance (Ω). Transepithelial voltages (V_{TE}) were calculated using Ohm's law.

$\Delta V = (\Delta I_{SC} * R_{TE})$

Tissues were continuously maintained at 37^{o}C and gassed with 5% CO_2-95% O_2 (pH:7.4). Mounted tissue was incubated for 30 minutes with 5 μM indomethacin and 1 μM tetrodotoxin to inhibit prostaglandin synthesis and potentially activated enteric neurons, respectively. Following equilibration, 10 μM amiloride was added apically to inhibit minor electrogenic Na^+ absorption (ENaC) in the distal colon. Upon reaching a steady-state, tissue was administered 100 μM carbachol (CCH) basolaterally to activate Gαq muscarinic receptors to indirectly activate apical Ca^{2+}-activated Cl^- secretion via intracellular increases in Ca^{2+} (11, 22). Fifteen minutes following CCH addition, 10 μM forskolin (FSK, adenylate cyclase inhibitor that increases intracellular cAMP) was basolaterally added to assess tissue viability. All representative traces and presented group data are designated as positive deflections indicating apical anion secretion/cation absorption or negative deflections representative of cation secretion/anion absorption.

Colonic Epithelial Cell Isolation. Distal colons were isolated from euthanized mice via bilateral pneumothorax and immediately rinsed with ice-cold phosphate-buffered saline (PBS) to clear luminal contents. The distal colon was then

opened longitudinally along the mesenteric border. Tissue was then cut into approximately 2 mm long pieces and submerged in 40 mL of ice-cold PBS with 5 mM EDTA in a 50 mL Falcon tube. The pieces of tissue in PBS-EDTA were then incubated at 37^{o}C with gentle rocking for 30 minutes. Following this incubation, colonic tissue was vigorously shaken to disperse colonic crypts and surface epithelium in solution. Supernatant was then loaded into 1.5 mL microcentrifuge tubes and spun at 1x10^{3} g for 5 minutes to pellet suspended cells. Isolated epithelial cells were used in downstream applications, such as RT-qPCR and Immunoblotting.

RNA Isolation and RT-qPCR analyses. Isolated colonic epithelium were resuspended in Qiazol (Qiagen, Valencia, Ca). Total-RNA was isolated using the MicroRNEasy kit, as per manufacturer's instructions (Qiagen, Valencia, Ca). Concentrated RNA was immediately quantified using the Nanodrop 1000 (Thermo, Waltham, MA). RNA was then stored at -80^{o}C until further application. Real-time PCR was carried out using a one-step kit that included 10 minutes of reverse transcription of total-RNA (50 ng/well) followed immediately by quantitative PCR utilizing a dsDNA-binding dye (New England Biolabs, Ipswich, MA). Custom primers (400 nM/primer/well) designed using the NCBI primer-blast application were utilized to amplify specific targets (Table-1). Determination of differential expression was achieved using the $2^{-\Delta\Delta Ct}$ method, (21). β-Actin threshold cycles for each sample were obtained and then subtracted from threshold cycles of transcripts of interest to obtain a ΔC_t value. The ΔC_t value

from control samples was then subtracted from DSS-colitis samples to obtain a $\Delta\Delta C_t$ value. Fold changes of transcripts of interest were then calculated as $2^{-_{\Delta\Delta}Ct}$ .This method was utilized for comparison of all quantitative PCR values presented within the text and figures.

Protein Isolation and Western Blotting. Pelleted colonic epithelium were resuspended in 350 µl of RIPA (radioimunnoprecipitation assay) buffer containing full protease inhibitor cocktail (cOmplete, Mini, Sigma-Aldrich, St. Louis, MO). Tissue was homogenized using glass homogenizers with a final sonication step to fully liberate transmembrane proteins. Protein concentration for each individual sample was determined using the Pierce BCA protein quantification kit (Thermo, Waltham, MA). Samples were then immediately frozen at -80^{o}C and maintained there until further use. On the day of immunoblotting, protein samples were removed from the -80^{o}C freezer and allowed to thaw on ice. Samples were diluted to 1 µg/µl with the addition of 4x Lammelli buffer (Biorad, Hercules, CA) and remaining volume with diH_2O. Following preparation, protein samples were warmed at 37^{o}C in a water bath for 15 minutes and then loaded at 20 µg/well onto handcast tris-glycine gels (SureCast, Invitrogen, Waltham, MA). Running conditions consisted of 85V until passing the stacking buffer at which point the gel was completed at 135V. Gels were transferred to PVDF membranes for 90 minutes at a constant 20V. Upon completion, PVDF membranes were blocked in 5% non-fat dry milk (Kroger, Cincinnati, OH) in tris-buffered saline with 0.1% tween-20 (TBST) for a period of 1 hour at room temperature. PVDF membranes

were then incubated in primary antibody: TMEM16A 1:500, CFTR 1:200, BEST2 1:500, M3R 1:200 (Alomone Labs, Jerusalem, Israel), IP3R 1:500, β-Actin 1:1000 (Cell Signaling, Danvers, MA) overnight at 4^{o}C. In the morning, membranes were washed 5x in TBST for 5 minutes and then placed in goat anti-rabbit horseradish-peroxidase conjugated secondary antibody (1:10000 dilution) for 2 hours at RT. Membranes were washed 5x in TBST and imaged on the G-Box (Syngene, Cambridge, United Kingdom). All target proteins were quantified using the imageJ software (National Institute of Health, Bethesda, MD) with normalization to β-Actin.

Statistics. All presented results represent mean ± standard error (SE) from five different animals, unless otherwise denoted. Statistical tests that were performed on the presented data sets were either unpaired student's t-test or one-way ANOVA with Tukey post-hoc analysis using GraphPad Prism 6.0 (San Diego, CA). $p < 0.05$ was used for determination of significance.

Stock Solutions. DSS (MP Biomedicals, Burlington, MA) 4% in the drinking water. Ussing chamber stock solutions were: 5 mM Indomethacin (Indo, dissolved in ethanol; Sigma-Aldrich, St. Louis, MO), 1 mM Tetrodotoxin (TTX, dissolved in acetic acid; Tocris Pharmaceuticals, Minneapolis, MN), 10 mM Amiloride (Amil, dissolved in DMSO; Sigma-Aldrich, St. Louis, MO), 100 mM Carbochol (CCH, dissolved in deionized water; Sigma-Aldrich, St. Louis, MO), 10 mM Forskolin (FSK, dissolved in DMSO; Tocris Pharmaceuticals, Minneapolis, MN), and 3 μM Ionomycin (IONO, dissolved in DMSO; Tocris Pharmaceuticals,

Minneapolis, MN). All stock solutions were diluted 1:1000 in the chamber to obtain [μM].

Results

Induction of Chronic DSS-colitis in Balb/c mice. Model accuracy was evaluated using several parameters previously utilized to demonstrate consistent induction of DSS-colitis (19). Colon length in the DSS-colitis group exhibited a consistent shortening as compared to control mice (Fig. 1A). Group data of measured colonic lengths from control mice were significantly longer than their DSS counterparts (8.75 ± 0.276 cm vs. 6.05 ± 0.221 cm, $p < 0.001$) (Fig. 1B). Histological studies were also conducted to examine proper colitis induction. The whole thickness of tissue isolated from control mice exhibited normal histological architecture (i.e. stacked test tubes) with intact surface epithelium and minimal inflammatory cells located in the lamina propria (Fig. 1C, top). Colonic mucosa from DSS-colitis animals exhibited substantial widening of the lamina propria as a result of an influx of inflammatory cells (Fig. 1C, bottom). Crypts in the colitic colon were also distorted with an obvious enlargement of the underlying muscularis (Fig. 1C, bottom), which could be the result of increased proliferation. However, this could also be the result of colonic contraction and without a marker for proliferation cannot be excluded. Transcript abundance of acute-phase reactants was quantitated to further demonstrate active inflammation within the distal colon. Quantitative PCR (qPCR) demonstrated a significant increase in cytokine transcript abundance of TNFα (1.008 ± 0.033 vs. 8.293 ± 0.732, $p < 0.0001$) and IL-6 (0.980 ± 0.017 vs. 10.530 ± 1.045, $p < 0.0001$) from DSS-colitis

samples (Fig. 1D). Besides the prototypical inflammatory cytokines, Th_2-mediated cytokines were selected for study for their relevance to the clinical pathology, UC. IL-17 mRNA abundance was not significantly increased (1.000 ± 0.754 vs. 2.964 ± 0.676), however, transcript abundance of IL-4 (1.506 ± 0.747 vs. 7.109 ± 2.229, $p < 0.05$), IL-10 (1.062 ± 0.144 vs. 11.310 ± 2.262, $p < 0.01$), and IL-33 (0.998 ± 0.028 vs. 4.340 ± 1.367, $p < 0.05$) were all significantly increased in the DSS-colitis mice (Fig. 1D).

Effect of Chronic DSS-induced Colitis on Ca^{2+}-activated Cl^- Secretion. Control mucosa demonstrated a robust increase in Ca^{2+}-activated Cl^- secretion, which was measured as positive deflections in short-circuit current (I_{SC}) (ΔI_{SC}, 15.40 ± 2.22 μA/cm^2, n = 5) (Fig. 2F). This was paralleled by a calculated hyperpolarization of transepithelial potential ($\Delta V_{TE,}$ -1.64 ± 0.21 mV, n=5) (Fig. 2E) following 100 μM CCH application (Fig. 2A/C). DSS-treated mucosa did elicit a response upon application of CCH, however, this response was significantly smaller in magnitude and opposite in apparent charge (Fig. 2B/D). The decrease in measured I_{SC} (ΔI_{SC}, -2.47 ± 0.25 μA/cm^2, n=5) (Fig. 2F) most likely indicates activation of Ca^{2+}-activated K^+ channels, which are known to reside in the apical membrane of colonic epithelium (31, 32, 36, 42). This altered response to basolateral CCH could potentially be related to decreased synthesis of prostaglandin E_2, which has previously been shown to uncouple CCH-administration from apical Cl^- secretion (7). Also, calculated V_{TE} paralleled this response with a slight depolarization due to increased positive charge accumulating on the luminal side of the chamber (ΔV_{TE}, 0.296 ± 0.07 mV, n = 5)

(Fig. 2E). Application of basolateral 10 μM Forskolin (FSK) was administered to assess the tissues ability to respond to another physiological agonist (Fig. 2C/D).

Effect of Acute DSS-induced Colitis on Ca^{2+}-activated Cl^- Secretion. Following our initial observations in the Ussing chamber that recapitulated previously published work with the acute model of DSS, along with western blot quantification of TMEM16A that demonstrated a decrease in expression (1.000 ± 0.13 vs. 0.065 ± 0.01, $p < 0.05$), we decided to utilize the acute model (16, 19). This was done to establish that changes in CCH-induced I_{SC} were in fact due to aberrations in intracellular Ca^{2+} responses. However, we first needed to establish that our acute model of DSS-induced colitis was in agreement with previously published literature (16). As previously seen with our controls from the chronic model, control mucosa elicited a robust increase in I_{SC} (ΔI_{SC}, 29.42 ± 6.42 μA/cm^2, n = 6) when exposed to basolateral 100 μM CCH (Fig. 3A/C). Also as expected, colonic mucosa isolated from animals that received DSS demonstrated a drop in baseline I_{SC} (ΔI_{SC}, -2.43 ± 0.17 μA/cm^2, n = 6) following basolateral 100 μM CCH (Fig. 3B/C). To then establish that Ca^{2+} mediates the CCH-induced changes in I_{SC} in control and DSS mucosa, 3 μM ionomycin (calcium ionophore, IONO) was added prior to basolateral CCH administration. 3 μM IONO induced an increase in measured I_{SC} in control mucosa (ΔI_{SC}, 15.30 ± 2.24 μA/cm^2, n = 4) (Fig. 3D/E), which was followed by basolateral addition of 100 μM CCH. Administration of CCH was only able to minimally increase I_{SC} (ΔI_{SC}, 0.90 ± 1.09 μA/cm^2, n = 4) (Fig. 3D/E). And when compared to mucosa that was treated with

CCH prior to IONO, the measured increase in I_{SC} was significantly less (ΔI_{SC}, 29.42 ± 6.42 μA/cm^2 vs. 0.90 ± 1.09 μA/cm^2, p< 0.01) (Fig. 3F). Colonic mucosa from DSS-colitis mice was then incubated with 3 μM IONO, which caused a drop in baseline I_{SC} (ΔI_{SC}, -3.21 ± 0.73 μA/cm^2, n = 4) (Fig. 3G/H). Following this, 100 μM CCH was administered to the basolateral surface of the tissue. CCH was only able to elicit a small drop in measured I_{SC} (ΔI_{SC}, -0.31 ± 0.49 μA/cm^2, n = 4) (Fig. 3G/H). Overall, this demonstrated a similar pattern to control mucosa of CCH-induced I_{SC} being attenuated when following IONO administration (ΔI_{SC}, -3.21 ± 0.73 μA/cm^2 vs. -0.31 ± 0.49 μA/cm^2, p< 0.01) (Fig. 3I). Taken together, these results would indicate that CCH-induced changes I_{SC} are Ca^{2+}-mediated in both control and DSS-exposed mucosa.

Effect of Chronic DSS-induced Colitis on Cl^- Channel Transcript Abundance. RT-qPCR analysis was utilized to assess transcript abundance of several Cl^- channels known to be expressed in distal colonic epithelium (28, 37, 41). Two Ca^{2+}-activated Cl^- channels (*Tmem16a, Best2*) as well as the cystic fibrosis transmembrane regulator (*Cftr*) were selected for analysis. *Tmem16a* mRNA abundance was significantly decreased in epithelium isolated from DSS-colitis mice (1.045 ± 0.15 vs 0.325 ± 0.04, p < 0.01) (Fig. 4A), which may indicate a potential decrease in translated channel protein. However, *Best2* (0.993 ± 0.03 vs. 0.301 ± 0.32, p < 0.001) and *Cftr* (1.042 ± 0.209 vs. 0.096 ± 0.013, p < 0.01) were also significantly decreased as compared to control animals (Fig. 4B/C).

Effect of Chronic DSS-induced Colitis on Cl^- Channel Protein Expression in Mucosal Lysates. Western blot of epithelial lysates focused on different Cl^- channels implicated to elicit a response to increasing intracellular levels of Ca^{2+} in colonic epithelium. Western blot technique was carried out on lysates to assess potential differences in protein expression between control and DSS mice. As previously seen with the RT-qPCR data, TMEM16A was significantly down-regulated in DSS-colitis (1.001 ± 0.13 vs. 0.510 ± 0.12, $p < 0.05$) (Fig. 5A/B). However, western blot quantification of BEST2, another CaCC, from the lysates demonstrated no difference between control and DSS groups (0.952 ±0.04 vs. 0.930 ± 0.031, $p > 0.05$) (Fig. 5A/C). CFTR was also quantified via western blot technique. This was to address previous observations that have described a mechanism by which CFTR is Ca^{2+}-sensitive (5, 38). Protein expression for CFTR was also unaltered (1.074 ± 0.09 vs. 1.053 ± 0.07, $p > 0.05$) (Fig. 5A/D) despite the mRNA transcript abundance being significantly decreased, similar to *Best2* (Fig. 4B/C).

Transcript and Protein Abundance of Gαq Muscarinic Signaling Pathway. Previous work has shown that the decreased CCH-stimulated I_{SC} in DSS-colitis was attributable to aberrations in signaling of pro-secretory stimuli (1, 18). To assess this from the standpoint of activation by CCH, mRNA abundance, as well as protein expression, of the M_3 receptor (CHRM3), a prototypical Gαq G-protein coupled receptor, was quantified in the distal colon. mRNA transcript abundance for *Chrm3* was unchanged between control and DSS-colitis groups (1.028 ± 0.12 vs. 1.029 ± 0.27, $p > 0.05$) (Fig. 6A). Western blot quantification of CHRM3 was

also unchanged between the different experimental groups (1.021 ± 0.24 vs. 0.928 ± 0.09, $p > 0.05$) (Fig. 6B/C). While signal transduction is initiated through CHRM3, canonical Gαq signaling also includes the production of the second messenger inositol triphosphate (IP_3), which leads to the release of Ca^{2+} via binding to the inositol triphosphate receptor (ITPR3). While *Itpr3* transcript abundance was not significantly decreased (0.988 ± 0.09 vs. 0.816 ± 0.05, $p > 0.05$), protein expression of ITPR3 was significantly down-regulated (1.000 ± 0.09 vs. 0.426 ± 0.13, $p < 0.01$) in DSS-colitis mice as compared to their parallel controls (Fig. 6A, B, D).

Immunohistochemistry of TMEM16A in Distal Colon of Control and DSS Mice. Immunohistochemistry (IHC) of TMEM16A was performed to follow-up the finding of decreased protein expression with immunoblotting (Fig. 5A/B) and to determine the exact localization of that protein. IHC performed with anti-TMEM16A antibody on control tissue demonstrated staining of the surface epithelium with additional staining of the upper crypts (Fig. 7A). However, DSS-exposed tissue that was incubated with anti-TMEM16A antibody demonstrated substantially less membrane staining of the epithelium, with more generalized staining of the cytoplasm (Fig. 7C). This generalized staining, especially in DSS-colitis, is most likely sub-apical vesicles that have not been properly trafficked to the plasma membrane, however, the staining could also be potential splice variants of TMEM16A located in cellular organelles. Control peptide experiments incubated with the anti-TMEM16A antibody were run in parallel for both groups. The addition of peptide to either Control or DSS-colitis tissue was devoid of

staining indicating specificity of the antibody, instead of possible non-specific binding to similar epitopes (Fig. 7B/D).

Discussion

Utilizing the previously described model of colitis in mice (20, 39), five alternating weeks of 4% DSS administration was able to induce epithelial dysplasia, crypt distortion and increased inflammatory infiltrate in the lamina propria, similar to the histopathological features observed in UC (2). Previously, acute induction of DSS-colitis had resulted in decreased CCH-stimulated Ca^{2+}-activated Cl^- secretion in murine distal colon (3, 16). However, these losses in Ca^{2+}-activated Cl^- secretion have been attributed to dysfunctional muscarinic receptor signaling (1), or membrane depolarization related to decreased functioning of basolateral K^+ channels (16). These previous works were also conducted prior to the discovery of the novel CaCC, TMEM16A (6, 34, 40). TMEM16A exhibits a similar electrophysiological profile to that found in cultured and native human bronchial epithelium (6). Also, global and tissue-specific knockout studies of TMEM16A in mice have demonstrated an absence of Ca^{2+}-activated Cl^- secretion (4, 28).

In this study, our findings demonstrate a significant attenuation in Ca^{2+}-activated Cl^- secretion in the colitic colon that is in part due to the down-regulation of TMEM16A. This conclusion is evidenced by the use of a Ca^{2+} ionophore (ionomycin) that demonstrates a complete lack of Ca^{2+}-activated Cl^- secretion (Fig. 3), as well as significantly decreased mRNA abundance and

protein expression of TMEM16A in the DSS-induced colitic colon (Figs. 4 & 5). In addition, other potential canonical and non-canonical CaCCs were also examined (5, 41). Transcript abundance was decreased for both *Best2* and *Cftr* (Fig. 4), however, the protein expression of these Cl^- channels in whole cell lysates was unchanged in the colitic colon, as compared to control littermates (Fig. 5). Also, transcript abundance and protein expression of CHRM3 were unchanged in DSS-induced colitis (Fig. 6), which is in agreement with a more recent publication (16). Taken together, our results indicate that decreased expression of TMEM16A following DSS administration substantially blunts Ca^{2+}-activated Cl^- secretion in murine distal colon.

While TMEM16A expression was substantially down-regulated, the protein expression of ITPR3 was also significantly decreased in the DSS-colitis cohort (Fig. 6). And while this could contribute to the attenuation in CCH-stimulated Cl^- secretion in DSS-colitis, a previous observation with a tissue-specific knockout of TMEM16A in colonic epithelium demonstrated decreased CCH-stimulated Ca^{2+} release as measured by fura-2 (33). Schreiber et al. did put forth one possibility that TMEM16A may provide a physical tether for ITPR3 to the plasma membrane and loss of TMEM16A could disrupt this architecture (33). Also, a prior study has demonstrated a physical interaction of TMEM16A and ITPR3 in nociceptive neurons (17). Taken together with our findings, the diminished expression of TMEM16A in colonic epithelium could cause a destabilization of ITPR3 in endoplasmic reticular membranes, leading to a premature degradation of the receptor. This notion is supported by the fact that mRNA abundance of *Itpr3*

(0.988 ± 0.09 vs. 0.816 ± 0.05, $p > 0.05$) is not significantly decreased in DSS-colitis (Fig. 6). This would potentially indicate a non-genomic mechanism of decreased protein expression, possibly a protein-protein interaction between ITPR3 and TMEM16A.

Though it is most likely that the down-regulation of TMEM16A is a result of transcriptional regulation, it is uncertain as to what mechanism mediates this regulation of the channel. Several groups have previously shown that IL-4 and IL-13, Th_2 immune mediators, were able to significantly increase Ca^{2+}-activated Cl^- secretion in bronchial epithelium (6, 43). Another group incubated IL-4 and IL-13 on immortalized colonic epithelium (T_{84}), and while IL-13 did not seem to have an effect, IL-4 was able to substantially inhibit the CCH-stimulated I_{SC} in a dose-dependent manner (23). Another study incubated IL-10 on T84 monolayers and was able to demonstrate a similar dose-dependent inhibition of CCH-stimulated I_{SC} (24). Together, this would provide support that Th_2 signaling in colonic epithelium may oppose the effects that are observed in respiratory epithelium. Also, it is worth noting that our results demonstrate a significant increase in transcript abundance of several prototypical Th_2 cytokines (Fig. 1D), which could lead to the decreased expression of TMEM16A.

Previous studies have demonstrated the importance for TMEM16A in mucociliary clearance in murine airways (28, 30). Furthermore, poor hydration of the mucus layer between secretory epithelium and resident bacteria has been shown to promote an environment of bacterial overgrowth, leading to an increased interaction of non-host with host (25, 27). This potentially highlights the

impact that TMEM16A may have on colonic inflammation in UC. Utilizing these previous observations, we speculate that decreased TMEM16A may exacerbate colonic inflammation via an increase in interaction between resident immune cells and the microbiota. From a clinical perspective an increase in Ca^{2+}-activated Cl^- secretion could decrease this interaction and help to ameliorate further inflammation induced via this mechanism.

In conclusion, our findings demonstrate a significant decrease in Ca^{2+}-activated Cl^- secretion in a DSS-induced colitic colon. The CaCC, TMEM16A, is significantly decreased in the DSS-induced colitis cohort of mice, while other Cl^- channels (BEST2, CFTR) were unchanged at the protein level. The significant decrease in ITPR3 may be the result of a loss of TMEM16A stabilization through protein-protein interactions. Also, we speculate that the loss of TMEM16A in colonic epithelium may contribute to the inflammatory response.

Acknowledgements

This study was supported by R01DK018777 (V.M. Rajendran) from the National Institute of Health/Diabetes and Digestive and Kidney Diseases.

Conflict of Interest

On behalf of all the authors, the corresponding author states that there is no conflict of interest.

References

1. **Akhtar M**, **Sayer B**, **Lu J**, **Green C**, **So JD**, **Mckay DM**. Dextran sodium sulphate-induced colitis perturbs muscarinic cholinergic control of colonic epithelial ion transport. *British Journal of Pharmacology* 135, 1794-1800.

2. **Appleman HD**. What Are the Critical Histologic Features in the Diagnosis of Ulcerative Colitis ?. *Inflammatory Bowel Disease* 14: 164–165, 2008.

3. **Ballester I**, **Zarzuelo A**. Disturbances in epithelial ionic secretion in different experimental models of colitis. *Life Sciences* 76: 1489–1501, 2005.

4. **Benedetto R**, **Ousingsawat J**, **Wanitchakool P**, **Zhang Y**, **Holtzman MJ**, **Amaral M**, **Rock JR**, **Schreiber R**, **Kunzelmann K**. Epithelial Chloride Transport by CFTR Requires TMEM16A. *Sci Rep* : 1–13, 2017.

5. **Billet A**, **Hanrahan JW**. The secret life of CFTR as a calcium-activated chloride channel. *J Physiol* 21: 5273–5278, 2013.

6. **Caputo A**, **Caci E**, **Ferrera L**, **Pedemonte N**, **Barsanti C**. TMEM16A, A Membrane Protein Associated with Calcium-Dependent Chloride Channel Activity. : *Science* 590–594, 2008.

7. **Carew MA**, **Thorn P**. Carbachol-stimulated chloride secretion in mouse colon: evidence of a role for autocrine prostaglandin E2 release. *Exp Physiol* 85: 67–72, 2000.

8. **Cheng SH**, **Gregory RJ**, **Marshall J**, **Paul S**, **Souza DW**, **White GA**, **D CF**, **Smith AE**. Defective Intracellular Transport and Processing of CFTR Is the Molecular Basis of Most Cystic Fibrosis. *Cell* 63: 827-834, 1990.

9. **Cliff WH**, **Frizzell RA**. Separate Cl- conductances activated by cAMP and Ca2 + in. *PNAS* 87: 4956–4960, 1990.

10. **Crowe SE**, **Luthra GK**, **Perdue MH**. Mast cell mediated ion transport in intestine from patients with and without inflammatory bowel disease. *Gut* 41: 785–792, 1997.

11. **Dharmsathaphorn K**, **Pandol SJ**. Mechanism of Chloride Secretion Induced by Carbachol in a Colonic Epithelial Cell Line. *Journal of Clin. Investigation* 77: 348-354, 1986 .

12. **Diaz-granados N**, **Howe K**, **Lu J**, **Mckay DM**. Dextran Sulfate Sodium-Induced Colonic Histopathology , but not Altered Epithelial Ion Transport , Is Reduced by Inhibition of Phosphodiesterase Activity. *American Journal of Patholgy* 156: 2169–2177, 2000.

13. **Dickinson KE**, **Frizzell RA**, **Sekar MC**. Activation of T84 cell chloride channels by carbachol involves a phosphoinositide-coupled muscarinic M3 receptor. *Eur J Pharmacol* 225: 291–298, 1992

14. **Sandle GI , Hayslett JP Binder HJ**. Effect of glucocorticoids on rectal transport in normal subjects and patients with ulcerative colitis. *Gut* 27 : 309–316, 1986.

15. **Galietta LJ V**. The TMEM16 Protein Family : A New Class of Chloride Channels ? *Biophysj* 97: 3047–3053, 2009.

16. **Hirota CL**, **Mckay DM**. Loss of Ca 2 + -mediated ion transport during colitis correlates with reduced ion transport responses to a Ca 2 + -activated K + channel opener. *British Journal of Pharmacology* 1085–1097, 2009.

17. **Jin X**, **Shah S**, **Liu Y**, **Zhang H**, **Lees M**, **Fu Z**, **Lippiat D**, **Beech DJ**, **Sivaprasadarao A**, **Baldwin SA**, **Zhang H**, **Gamper N**. Europe PMC Funders Group Activation of the Cl − Channel ANO1 by Localized Calcium Signals in Nociceptive Sensory Neurons Requires Coupling with the IP_3 Receptor. *Science Signal.* 6, ra73 2013.

18. **Kachur JF**, **Keshavarzian A**, **Sundaresan R**, **Doria M**, **Walsh R**, **de las Alas MM**, **Gaginella TS**. Colitis reduces short-circuit current response to inflammatory mediators in rat colonic mucosa. *Inflammation* 19: 245–259, 1995.

19. **Kanthesh BM**, **Sandle GI**, **Rajendran VM**. Enhanced K(+) secretion in dextran sulfate-induced colitis reflects upregulation of large conductance apical K(+) channels (BK; Kcnma1). *Am J Physiol Cell Physiol* 305: C972-80, 2013.

20. **Kim JJ**, **Shajib S**, **Manocha MM**, **Khan WI**. Investigating Intestinal Inflammation in DSS-induced Model of IBD. : *J. Vis. Exp. (60): e3678,*

2012.

21. **Livak KJ**, **Schmittgen TD**. Analysis of Relative Gene Expression Data Using Real- Time Quantitative PCR and the $2^{-\Delta\Delta}$ C T Method. *Methods* 25: 402–408, 2001.

22. **Luo D**, **Broad LM**, **Bird GSJ**, **Putney JW**. Signaling Pathways Underlying Muscarinic Receptor-induced [Ca 2+]i Oscillations in HEK293 Cells. *J Biol Chem* 276: 5613–5621, 2001.

23. **Madara JL**, **Dzus AL**, **Awtrey CS**, **Colgan SP**. Interleukin-4 and Interleukin-13 Differentially Regulate Epithelial Chloride Secretion *. *The Journal of Biological Chemistry* 271: 7460–7464, 1996.

24. **Madsen KL**, **Lewis SA**, **Tavernini MM**, **Hibbard J**, **Fedorak RN**. Interleukin 10 prevents cytokine-induced disruption of T84 monolayer barrier integrity and limits chloride secretion. *Gastroenterology* 113: 151–159, 1997.

25. **Malin E.V. Johansson, Henrik Sjövall and GCH**. The gastrointestinal mucus system in health and disease. *Nat Rev Gastroenterol Hepatol* 10: 352–361, 2013.

26. **Nanda Kumar NS**, **Singh SK**, **Rajendran VM**. in colon secretion provides the driving force for electrogenic anion Mucosal potassium efflux mediated via Kcnn4 channels Mucosal potassium efflux mediated via Kcnn4 channels provides the driving force for electrogenic anion secretion in

colon. *Am J Physiol Gastrointest Liver Physiol* 299: 707–714, 2010.

27. **Norkina O**, **Burnett TG**, **Lisle RC De**. Bacterial Overgrowth in the Cystic Fibrosis Transmembrane Conductance Regulator Null Mouse Small Intestine. *Infection and Immunity* 72: 6040–6049, 2004.

28. **Ousingsawat J**, **Martins JR**, **Schreiber R**, **Rock JR**, **Harfe BD**, **Kunzelmann K**. Loss of TMEM16A Causes a Defect in Epithelial Ca^{2+} -dependent Chloride Transport *. *The Journal of Biological Chemistry* 284: 28698–28703, 2009.

29. **Rock JR**, **Futtner CR**, **Harfe BD**. The transmembrane protein TMEM16A is required for normal development of the murine trachea. *Developmental Biology* 321: 141–149, 2008.

30. **Rock JR**, **Neal WKO**, **Gabriel SE**, **Randell SH**, **Harfe BD**, **Boucher RC**, **Grubb BR**. Transmembrane Protein 16A (TMEM16A) Is a Ca^{2+} -regulated Cl^- Secretory Channel in Mouse Airways *. *The Journal of Biological Chemistry* 284: 14875–14880, 2009.

31. **Sandle GI**, **Rajendran VM**. Cyclic AMP-induced K+ secretion occurs independently of Cl- secretion in rat distal colon. *Am J Physiol Cell Physiol* 303: C328-33, 2012.

32. **Sausbier M**. Distal Colonic K+ Secretion Occurs via BK Channels. *J Am Soc Nephrol* 17: 1275–1282, 2006.

33. **Schreiber R**, **Faria D**, **Skryabin B V.**, **Wanitchakool P**, **Rock JR**, **Kunzelmann K**. Anoctamins support calcium-dependent chloride secretion by facilitating calcium signaling in adult mouse intestine. *Pflugers Arch Eur J Physiol* 467: 1203–1213, 2015.

34. **Schroeder BC**, **Cheng T**, **Jan YN**, **Jan LY**. Expression cloning of TMEM16A as a calcium-activated chloride channel subunit. *Cell* 134: 1019–1029, 2008.

35. **Scudieri P**, **Caci E**, **Bruno S**, **Ferrera L**, **Schiavon M**, **Sondo E**, **Tomati V**, **Gianotti A**, **Zegarra-moran O**, **Pedemonte N**, **Rea F**, **Ravazzolo R**, **Galietta LJ V**. Association of TMEM16A chloride channel overexpression with airway goblet cell metaplasia. *J Physiol* 23: 6141–6155, 2012.

36. **Sorensen M V.**, **Matos JE**, **Praetorius HA**, **Leipziger J**. Colonic potassium handling. *Pflugers Arch Eur J Physiol* 459: 645–656, 2010.

37. **Thiagarajah JAYR**, **Broadbent T**, **Hsieh E**, **Verkman AS**. Prevention of Toxin-Induced Intestinal Ion and Fluid Secretion by a Small-Molecule CFTR Inhibitor. *Gastroenterology 126: 511-519,* 2004.

38. **Wan Namkung, Walter E. Finkbeiner and ASV**. CFTR-Adenylyl Cyclase I Association Responsible for UTP Activation of CFTR in Well-Differentiated Primary Human Bronchial Cell Cultures. *Mol Biol Cell* 21: 4042–4056, 2010.

39. **Wirtz S**, **Neufert C**, **Weigmann B**, **Neurath MF**. Chemically induced

mouse models of intestinal inflammation. *Nature Protocols* 2: 541–546, 2007.

40. **Yang YD**, **Cho H**, **Koo JY**, **Tak MH**, **Cho Y**, **Shim W**, **Park SP**, **Lee J**, **Lee B**, **Kim B**, **Raouf R**, **Shin YK**, **Oh U**. TMEM16A confers receptor-activated calcium-dependent chloride conductance. *Nature* 455: 1210–1216, 2008.

41. **Yu K**, **Lujan R**, **Marmorstein A**, **Gabriel S**, **Hartzell HC**. Bestrophin-2 mediates bicarbonate transport by goblet cells in mouse colon. *The Journal of Clinical Investigation* 120: 1722-1735, 2010.

42. **Zhang J**, **Halm ST**, **Halm DR**. Role of the BK channel (KCa1.1) during activation of electrogenic K+ secretion in guinea pig distal colon. *AJP Gastrointest Liver Physiol* 303: G1322–G1334, 2012.

43. **Zhang Y**, **Wang X**, **Wang H**, **Jiao J**, **Li Y**, **Fan E**, **Zhang L**, **Bachert C**. TMEM16A-Mediated Mucin Secretion in IL-13-Induced Nasal Epithelial Cells From Chronic Rhinosinusitis Patients. *Allergy Asthma Immuno Res* 7: 367–375, 2015.

Figure Legends

Figure 1. **Evaluation of DSS-colitis in Balb/C Mice**. *A.* Representative images of excised colons from either control or DSS-colitis cohorts. *B.* Group data of measured colons from either control or colitic mice. Represented data is means ± SE of different groups, collected from 6 different animals in each respective group ($p < 0.001$). *C*. Haemotoxylin and eosin staining of formalin-fixed colonic tissue. Each image represents a different animal from their corresponding treatment. DSS-colitis (C, Bottom) demonstrates crypt dysplasia, leukocyte infiltration, and thickening of underlying serosa (20x, AxioImager). *D.* RT-qPCR analyses of multiple cytokines involved in the development of colitis. Asterisks (*) indicate significance of each individual cytokine transcript as compared to control. *$p < 0.0001$ – compared to control; \$$p < 0.01$ – compared to control; #$p < 0.05$ – compared to control.

Figure 2. **Effect of DSS-colitis on transepithelial potential and Cl^- secretion**. *A.* Representative trace of calculated transepithelial potential (V_{TE}) in control mice following application of 100 μM carbochol (CCH) and 10 μM Forskolin (FSK). *B.* Representative trace of calculated V_{TE} in DSS-colitis mice following application of 100 μM CCH and 10 μM FSK. *C.* Representative trace of elicited short-circuit current (I_{SC}) in control mice following basolateral administration of 100 μM CCH and 10 μM FSK. *D.* Representative trace of elicited I_{SC} in DSS-colitis mice following basolateral administration of 100 μM CCH and 10 μM FSK. *E.* Summarized data of calculated ΔV_{TE} following CCH administration in either

control (open bars) or DSS-colitis (closed bars) mice. DSS-colitis demonstrates a complete inhibition with an actual reversal in polarity as compared to control. *F.* Group data of ΔI_{SC} from both control (open bars) and DSS-colitis (closed bars) groups following CCH-administration. DSS-colitis, in parallel to calculated ΔV_{TE}, demonstrates an elicited current that is in opposition to that of the control cohort. Bar graphs of summarized data represent means ± SE of 5 different animals. *$p < 0.001$ - compared to control.

Figure 3. **Effect of Ionomycin on CCH-induced Changes in I_{SC} from Control and Acute DSS-Colitis Mice.** *A.* Representative trace of measured short-circuit current (I_{SC}) following basolateral 100 μM carbochol (CCH) administration to control mucosa. *B.* Representative trace of I_{SC} from DSS-colitis mucosa following basolateral 100 μM CCH administration. *C.* Group data of ΔI_{SC} following CCH-administration in control and DSS mice. *D.* Representative trace of I_{SC} from control mucosa that was stimulated with 3 μM ionomycin (IONO) and followed by 100 μM CCH. *E.* Group Data of ΔI_{SC} with 3 μM IONO followed by 100 μM CCH in control mucosa. *F.* Group data of CCH-induced ΔI_{SC} with and without 3 μM IONO administration. *G.* Representative trace of I_{SC} from mucosa exposed to DSS administered 3 μM IONO and 100 μM CCH. *H.* Group data of ΔI_{SC} from DSS-colitis in response to 3 μM IONO followed by 100 μM CCH administration. *I.* Group data of DSS-colitis CCH-induced ΔI_{SC} with and without 3 μM IONO administration. All presented bar graphs are summarized data that represent the means ± SE. *$p < 0.01$ – compared to control.

Figure 4. **Effect of DSS-colitis on transcript abundance of Cl^- channels in murine colon**. Transcript abundance was determined for (A) *Tmem16a*, (B) *Best2*, and (C) *Cftr* in control (open bar) or DSS-colitis mice (closed bar). Bar graphs of summarized data represent means ± SE of 5 different animals normalized to an endogenous control, *Actb*. *$p < 0.001$ - compared to their respective control.

Figure 5. **Effect of DSS-colitis on Cl^- channel protein expression in murine colon**. *A.* Representative images of protein expression of the different characterized Cl^- channels from epithelial lysates. *B.* TMEM16A protein expression normalized to β-actin for quantification of control and DSS-colitis groups. TMEM16A expression (closed bars) is significantly decreased in DSS-colitis mice as compared to control. *C,D.* Summarized data of western blot quantification of BEST2 and CFTR normalized to β-actin in control and DSS-colitis mice. Neither protein was significantly altered from the control cohort. Bar graphs of summarized data represent means ± SE of 5 different animals from each respective group. *$p < 0.05$-compared their respective control.

Figure 6. **Characterization of Gαq muscarinic signaling pathway**. *A.* Transcript abundance of *Chrm3* and *Itpr3* from control and DSS-colitis groups. mRNA abundance of either transcript was not significantly different from the control cohort ($P>0.05$). *B.* Representative images of western blots for CHRM3

and ITPR3 with corresponding loading controls for normalization. *C.* Summarized data of CHRM3 protein expression normalized to β-actin. CHRM3 expression in DSS-colitis was unaltered as compared to control counterparts. *D.* Group data of ITPR3 protein expression normalized to β-actin from control and DSS-colitis. ITPR3 expression was significantly down-regulated in DSS-colitis. Bar graphs of summarized data represent means ± SE of 5 different animals from each respective group. *$p < 0.01$-as compared to control.

Figure 7. **Immunohistochemistry of TMEM16A in colonic tissue sections**. *A.* Immunohistochemistry of TMEM16A in control tissue demonstrates pronounced expression and localization of the protein to surface epithelium and upper crypts (top, left). *B.* DSS-colitis tissue stained for TMEM16A exhibits less staining in epithelial cells and a more diffuse signal in the lamnia propria (Bottom, left). *C,D.* Both cohorts of tissue were run in parallel with a control peptide specific for the anti-TMEM16A antibody. Both images demonstrate a lack of staining when co-incubated with control peptide. Images were captured at 20x magnification on the AxioImager (Carl Zeiss, Germany).

GENE ID (ref seq)	PRIMERS (Forward & Reverse)	Product Length (bp)	MELTING TEMP (^{o}C)
Tmem16a NM_178642.5	F: TCTGTGTTTATGGCCCTCTGG R: TGACAGCTTCCTCCTCCTCC	115	F: 59.72 R: 60.62
Best2 NM_001130194.1	F: CCGCCTATCGCTTCTTACTGG R: GATGCACCACCAGAGTCACG	132	F: 60.60 R: 61.02
Cftr NM_021050.2	F: ATTTCACGCTCCACAGAGGC R: CCATTAACGGGGTTGTTTTTAAGC	118	F: 60.67 R: 59.31
Chrm3 NM_033269.4	F: CTGCCAGATATGACCAGCAATGG R: TCACTTGGTCAGAACGCAGC	141	F: 61.61 R: 60.88
Itpr3 NM_080553.3	F: ACATTGTGTCCCTGTACGCC R: CACTTTGAAGAGGCAATCTCGG	143	F: 60.32 R: 59.58

Table 1. **Custom qPCR primers for determination of transcript abundance**. All primers were designed utilizing the NCBI primer-blast application with the indicated reference sequence (ref seq).

Figure 1.

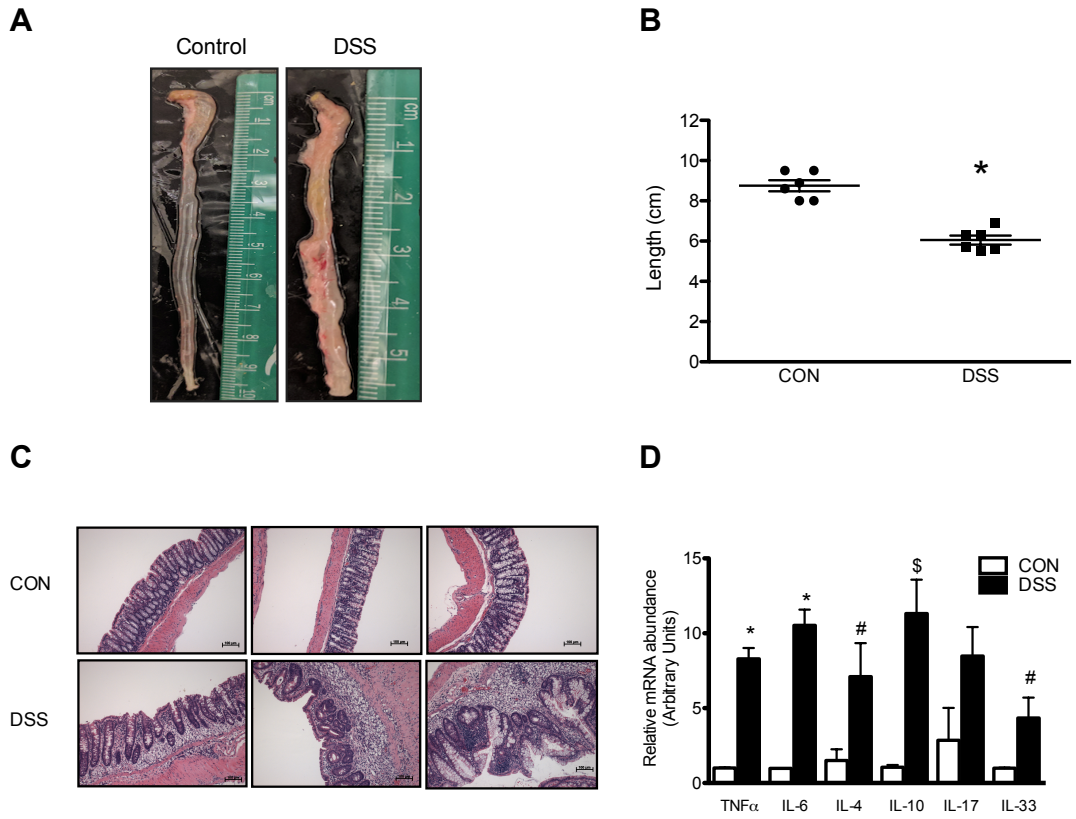
A
Control
DSS
B
Length (cm)
12
10
8
6
4
2
0
*
CON
DSS
C
CON
DSS
D
Relative mRNA abundance (Arbitrary Units)
15
10
5
0
CON
DSS
*
*
#
$
#
TNFα
IL-6
IL-4
IL-10
IL-17
IL-33

Figure 2.

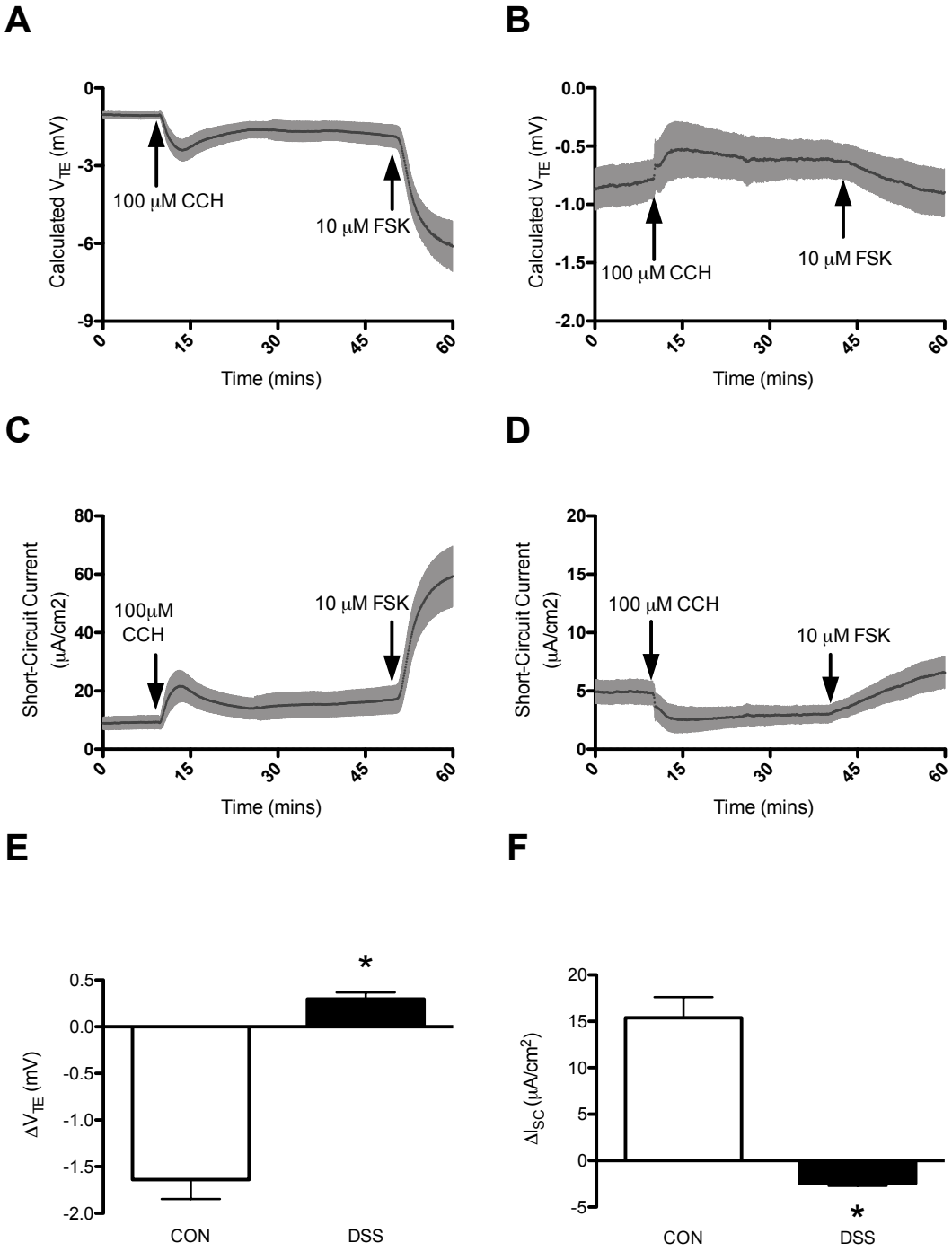
A
B
C
D
E
F
Calculated V_{TE} (mV)
100 μM CCH
10 μM FSK
Time (mins)
Short-Circuit Current (μA/cm2)
100μM CCH
ΔV_{TE} (mV)
ΔI_{SC} (μA/cm^2)
CON
DSS
*

Figure 3.

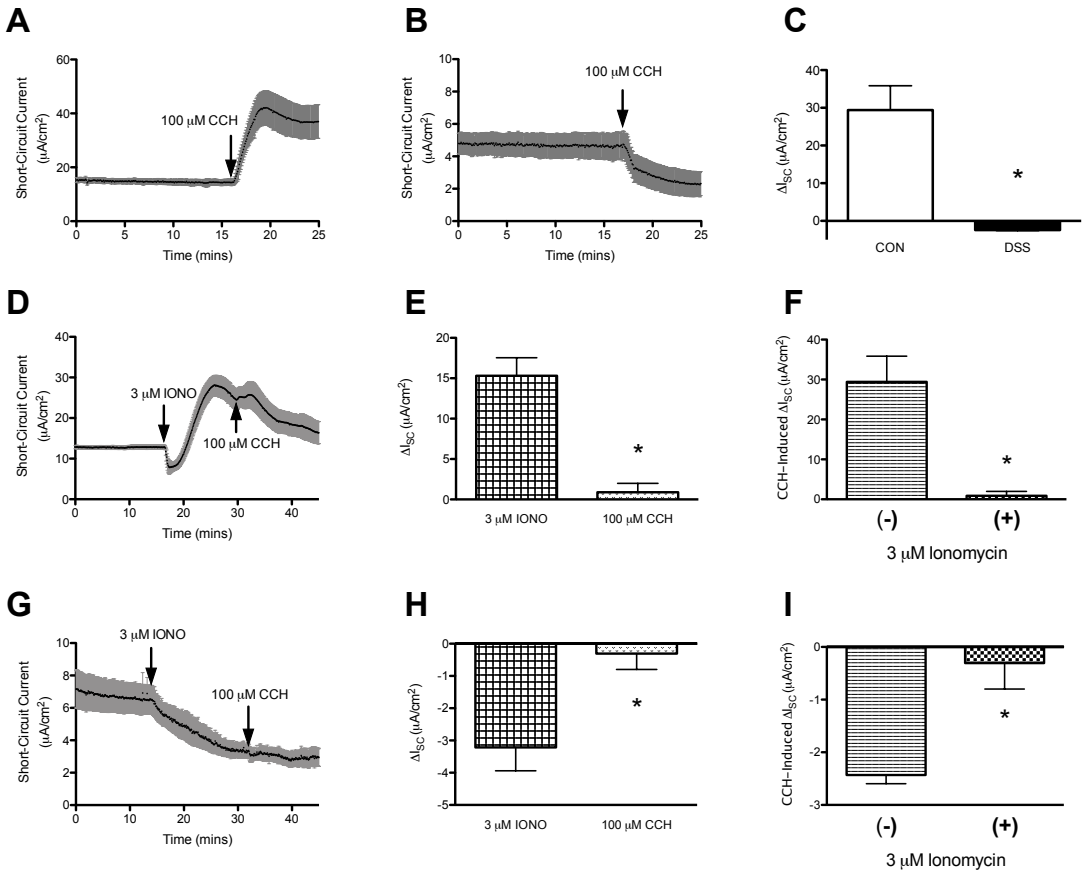
A
B
C
D
E
F
G
H
I
Short-Circuit Current (μA/cm²)
Time (mins)
100 μM CCH
3 μM IONO
ΔISC (μA/cm²)
CON
DSS
3 μM IONO
100 μM CCH
CCH-Induced ΔISC (μA/cm²)
(-)
(+)
3 μM Ionomycin

Figure 4.

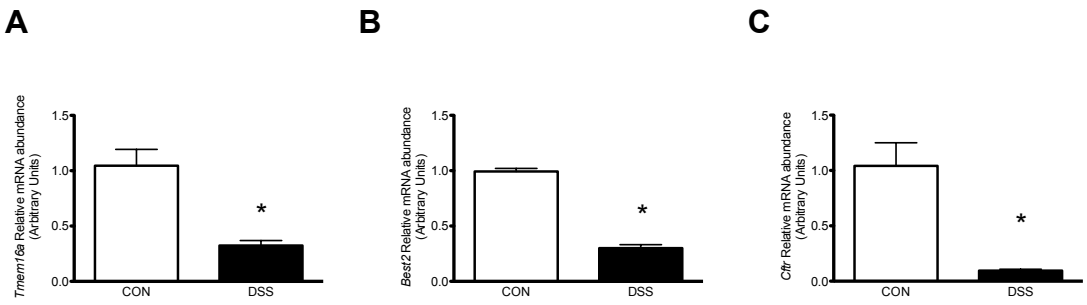
A
B
C
Tmem16a Relative mRNA abundance (Arbitrary Units)
Best2 Relative mRNA abundance (Arbitrary Units)
Cftr Relative mRNA abundance (Arbitrary Units)
1.5
1.0
0.5
0.0
*
CON
DSS

Figure 5.

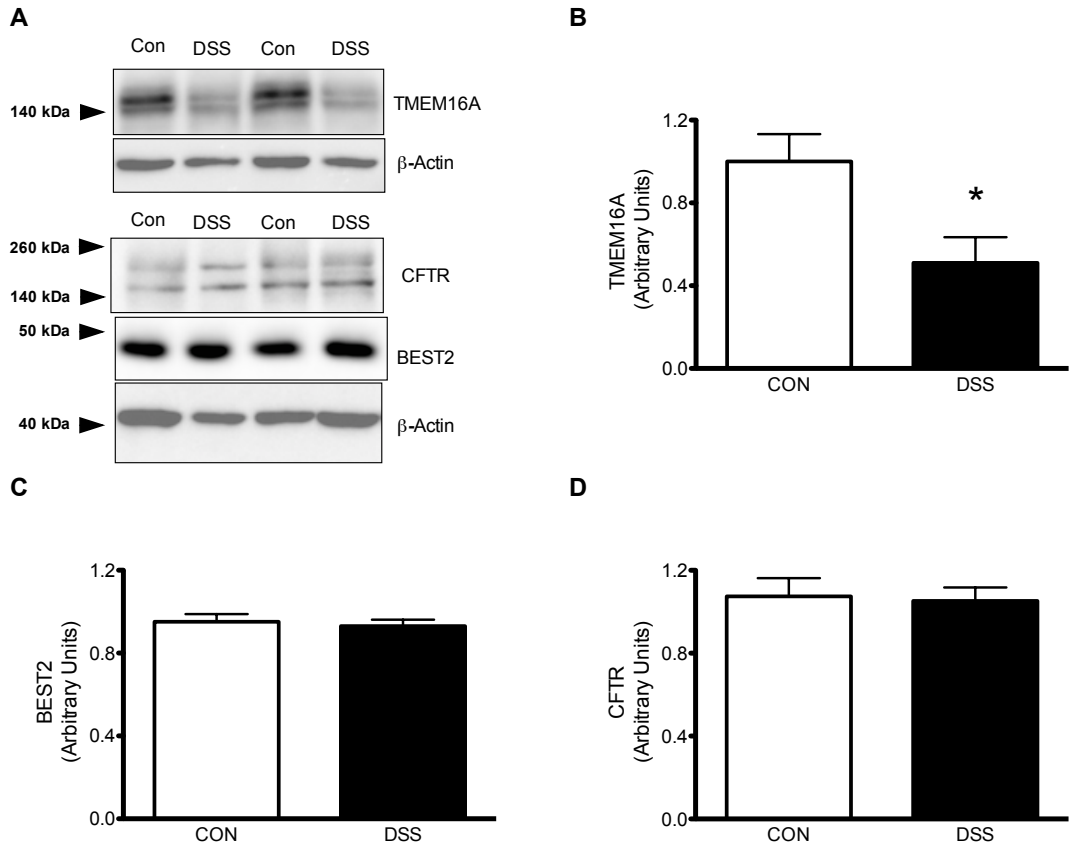
A
Con
DSS
Con
DSS
140 kDa
TMEM16A
β-Actin
Con
DSS
Con
DSS
260 kDa
140 kDa
50 kDa
CFTR
BEST2
40 kDa
β-Actin
B
TMEM16A (Arbitrary Units)
1.2
0.8
0.4
0.0
*
CON
DSS
C
BEST2 (Arbitrary Units)
1.2
0.8
0.4
0.0
CON
DSS
D
CFTR (Arbitrary Units)
1.2
0.8
0.4
0.0
CON
DSS

Figure 6.

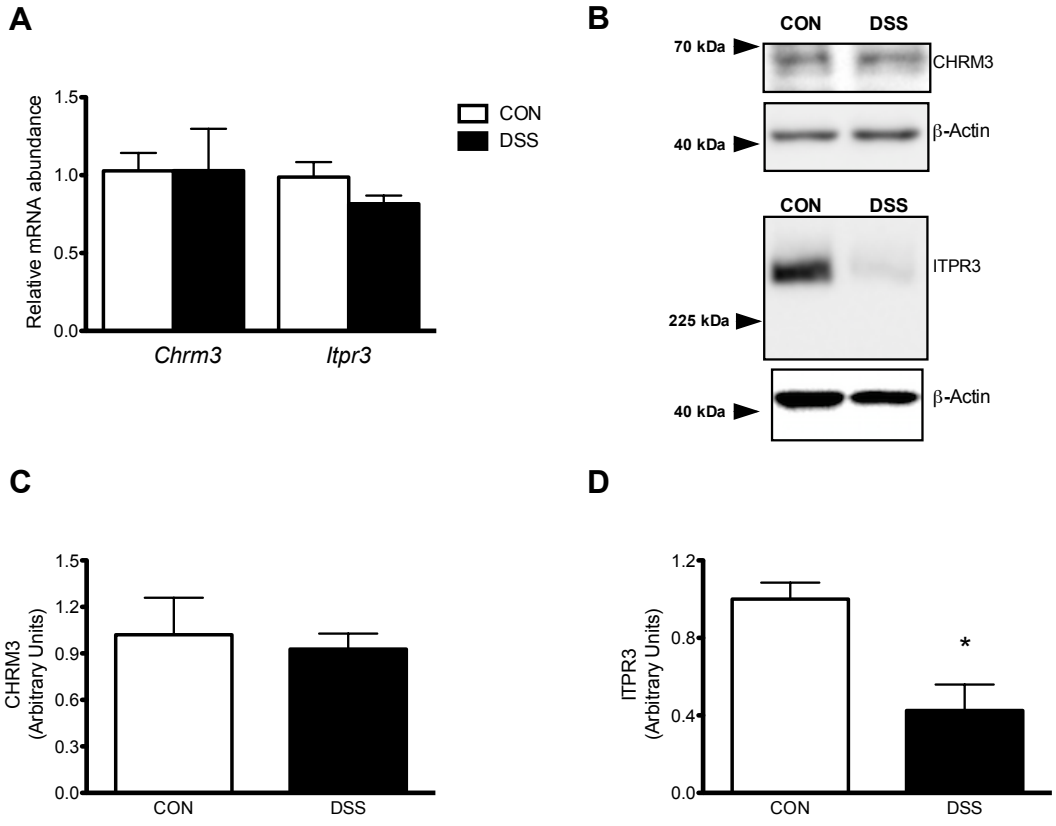
A
Relative mRNA abundance
1.5
1.0
0.5
0.0
CON
DSS
Chrm3
Itpr3
B
CON
DSS
70 kDa
CHRM3
40 kDa
β-Actin
CON
DSS
ITPR3
225 kDa
40 kDa
β-Actin
C
CHRM3
(Arbitrary Units)
1.5
1.2
0.9
0.6
0.3
0.0
CON
DSS
D
ITPR3
(Arbitrary Units)
1.2
0.8
0.4
0.0
*
CON
DSS

Figure 7.

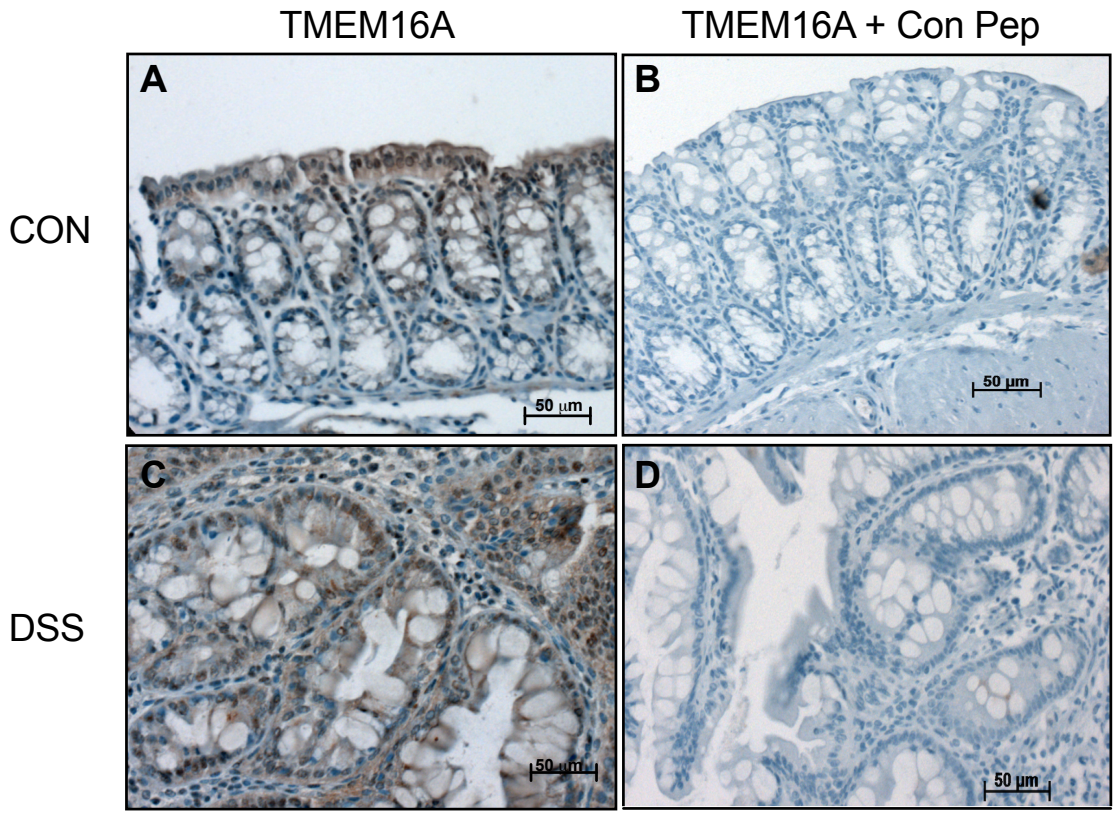

Chapter III

Activation of KCNQ (K_V7) K^+ Channels in Enteric Neurons Inhibits Chloride Secretion in the Murine Distal Colon

Trey S. Rottgen[1,*2], Andrew J. Nickerson[1,2], and Vazhaikkurichi M. Rajendran[1,2,*]

[1]Department of Physiology, Pharmacology, and Neuroscience, West Virginia University School of Medicine, Morgantown, West Virginia
[2]Department of Biochemistry and Molecular Pharmacology, West Virginia University School of Medicine, Morgantown, West Virginia

Running Title: K_V7 Activation Inhibits Colonic Secretion via Enteric Neurons

Key Words: Ussing Chamber, Colonic epithelium, KCNQ, K_V7 channels, Enteric neurons,

Abstract. The Enteric nervous system (ENS) regulates blood flow, motility and electrolyte transport along the entire gastrointestinal tract. KCNQ K^+ channels have been characterized to contribute to the resting membrane potential in visceral neurons and are also present in the ENS. In this study, we wanted to evaluate the efficacy of KCNQ activators on the ENS from the standpoint of anion secretion in mouse distal colon. Anion (i.e. Cl^-) secretion was measured as a function of short circuit current (Isc) in intact mouse distal colon mounted under voltage clamp conditions in an Ussing chamber. Pharmacological approaches were utilized to assess the effect of activation of KCNQ channels in enteric neurons on apical Cl^- secretion. Immunofluorescence studies were conducted to identify the isoform and location specific expression of KCNQ channels. Immunofluorescence studies indicated the presence of $K_V7.2$ and $K_V7.3$ channels that co-localized with choline acetyl transferase in enteric neurons of mouse distal colon. Flupirtine, a KCNQ activator markedly inhibited I_{SC} (i.e. Cl^- secretion). However, application of flupirtine following tetrodotoxin resulted in a significantly blunted response. A similar effect was observed when tissue was pre-incubated with the muscarinic antagonist tolterodine. Serosal nicotine stimulated Cl^- secretion in control colon. However, tissues that were pretreated with flupirtine prior to application of nicotine remained unresponsive to the ganglionic agonist. Our data indicate that activation of KCNQ (K_V7) channels of enteric neurons inhibits Cl^- secretion. Also, activators of KCNQ channels could have therapeutic benefit in diarrheal pathologies associated with an overall hyperexcitable ENS.

Introduction

The enteric nervous system (ENS) is comprised of approximately 400-600 million neurons [1]. The ENS participates in a multitude of functions that include regulation of motility, local control of blood flow during digestion, and influence over electrolyte transport [2-5].

Numerous pathologies have been identified that cause a dysregulation of one or all of the previously mentioned regulatory processes [6-8]. While Hirschprung's disease is the most notable of ENS pathologies, and results in an absolute loss of enteric neurons, several diseases have been identified that elicit an overall hyperexcitable ENS [9, 10]. For example, patients with irritable bowel syndrome with diarrhea (IBS-D) administered alosetron demonstrated delayed colonic transit times, indicating increased serotonergic signaling and ENS overactivity [9]. While IBS-D is considered more of a disease of the developed world, infections with rotavirus or *vibrio* cholera can also cause excitation of enteric neurons, which could increase epithelial secretion and contribute to the overall pathology of each of those diseases [8, 11].

K^+ channels are responsible for setting the resting membrane potential in a vast array of cells due to the large permeability of K^+ as compared to other predominant ions [12]. The KCNQ (K_V7) family, which are voltage-sensitive K^+ channels (K_V), have been described to regulate resting membrane potential in several different cell types [13-15]. The K_V7 family has been described as small, slow-deactivating K^+ channels with a hyperpolarized threshold for half-maximal activation [16]. A couple members of the K_V7 family, $K_V7.2$ and $K_V7.3$, have been

characterized as making up the native M current, and more importantly contributing to resting membrane potential in neurons [17-20]. Disruptions in these genes have led to the development of seizures and hyperalgesia in rodent models [19, 21, 22]. Previous observations have also shown $K_V7.3$ to co-immunolocalize with sensory afferents in the gastrointestinal tract, as well as, participate in visceral nociception [18, 23].

While the K_V7 family has been shown to be present in neurons located within the gastrointestinal tract, it has not previously been studied from the aspect of epithelial electrolyte transport. Therefore, the goal of this study was to evaluate the efficacy of K_V7 activators on enteric neurons and the resultant effect on mucosal electrolyte transport. Our results indicate that $K_V7.2/3$ activation causes an immediate and sustained hyperpolarization of enteric neurons that results in decreased epithelial secretory function via decreased neurotransmitter release.

Material and Methods

Animals. Male Balb/c mice (10-13 weeks, Charles River, NY) were provided normal chow and water ad libitium for the entirety of the project. All animals were anesthetized via 5% inhalational isoflurane (Patterson Veterinary, SC) for isolation of the whole colon for downstream applications. Mice were then euthanized via cervical dislocation. All experimental protocols utilized in this study were approved by the West Virginia University Institutional Animal Care and Use Committee.

Cell Culture. The colonic adenocarcinoma T_{84} cell line (ATCC, Manassas, VA) was maintained and passaged in a T75 flask (Corning, Corning, NY) that was kept at 37^{o}C and 5% CO_2- 95% O_2 gas. Cells were maintained in DMEM/F12 (ThermoFisher, Waltham, MA) supplemented with 10% fetal bovine serum (FBS) (Fisher Scientific, Hampton, NH) with 1% pencillin-streptomycin (Mediatech, Manassas, VA). Upon passage, cells were seeded close to confluence on 1.12 cm^2 transwell plates (Corning, Corning, NY) for use in Ussing chamber monolayer studies. T_{84} cells maintained on the transwell plates were checked for confluence each day. Upon reaching confluence, cells were then maintained in monolayers for 18 days for proper development of tight junctions, as well as, differentiation of the colonic epithelial cell line. Media was replaced every other day with fresh culture media until utilization in Ussing chamber studies.

Electrophysiology.

Native tissue. Whole colon was removed from the anesthetized mouse and rinsed with ice-cold phosphate-buffered saline (PBS) to remove any residual contents. Whole colon was then pinned near the caecum in a sylgard plate filled with ice-cold PBS containing 5 μM indomethacin. The colon was then opened longitudinally along the mesenteric border of the tissue. The sylgard dish was then placed under a dissecting microscope for the isolation of distal colon segments. Whole-mount distal colon was then placed on an oval 0.04 cm^2 aperture for mounting in the EasyMount Ussing chamber (Physiological Instruments, San Diego, CA) for electrophysiological study, as previously described [24]. Mounted tissue was then bathed with bilateral addition of 5 mL of Ringers' physiological saline solution (in mM: 115 NaCl, 25 $NaHCO_3$, 2.4 K_2HPO_4, 0.4 KH_2PO_4, 3 KCl, 1.2 $CaCl_2$, 1.2 $MgCl_2$ and 10 glucose) to each hemi-chamber. Tissues were allowed to equilibrate in open-circuit conditions for a period of 15 minutes prior to voltage-clamping. All mounted tissues were continuously voltage-clamped at 0 mV to abolish any developing electrical gradient. Short-circuit current (I_{sc}) was continuously monitored with a 5 mV pulse applied every 5 seconds to determine transepithelial resistance. Tissues were maintained in the chamber at 37°C and continuously gassed with 5% CO_2- 95% O_2 (pH 7.4).

T_{84} monolayers. The day of experiments, PBS was warmed in a water bath to 37°C for washing of T_{84} monolayers maintained on transwell plates. Inserts of T_{84} cells were removed from their respective plates and gently washed with warmed

PBS until clear. Monolayers were then mounted in the EasyMount Ussing chamber and bathed on both sides by Ringers' physiological saline solution. Monolayers were voltage-clamped at 0 mV for the duration of the experiment with a 5 mV pulse applied every 5 seconds. However, all monolayers were allowed to equilibrate and come to a steady-state prior to the application of any drugs.

All representative traces presented within this article are designated as positive I_{SC} indicating either secretion of an anion or absorption of a cation from the mucosal surface, while negative deflections of I_{SC} indicate cation secretion or anion absorption from the mucosal side of the tissue.

Immunofluorescence. Whole colon was removed from euthanized mice and rinsed with ice-cold PBS to remove any residual contents. Tissues were pinned on a sylgard plate and opened longitudinally along the mesenteric border. Colon was then pinned along the borders with the mucosa facing up. A shallow, longitudinal cut was made to remove mucosa from the underlying myenteric plexus and smooth muscle. Mucosa was then carefully teased away, starting from the cut and moving proximally along the colon. Upon isolation of the myenteric plexus and longitudinal smooth muscle, tissues were placed in 10% neutral-buffered formalin for 2 hours at RT. Following fixation, tissue was placed in 30% sucrose solution dissolved in PBS and stored at 4^{o}C until further processing. The day of immunostaining, tissue was removed from sucrose solution and washed 3x with PBS for a period of 1 hour to rehydrate the tissue.

Tissue was then incubated with 1% Triton-X100 PBS for a period of 4 hours to fully permeabilize the membranes. Samples were then washed with PBS 3x for 10 minutes and placed in 5% goat serum to block for 2 hours. Following blocking, tissue was placed in the different primary antibodies (K_V7.2 1:100, K_V7.3 1:100, Alomone Labs, Jerusaleum, Israel, ChAT 1:100 Millipore, Burlington, MA) diluted in blocking solution overnight at 4^oC with gentle shaking. In the morning, tissue was washed with PBS at RT 5x for 5 minutes. Upon completion of washing, tissue was incubated with secondary antibody (anti-rabbit Alexa Fluor 488 1:500, anti-goat Alexa Fluor 546 1:500) for 4 hours in the dark at RT. Tissue was removed and washed with PBS 5x for 5 mins to dilute out any residual secondary antibody. Samples were then mounted on slides with mounting media (Slowfade Diamond, ThermoFisher, Waltham, MA) and imaged for immunolocalization accordingly. All images were captured on LSM 510 confocal microscope (Carl Zeiss, Oberkochen, Germany) with a 63x oil-immersion objective.

Percent Inhibition and Dose-Response.

Percent inhibition. The percent inhibition of the different drugs was calculated by obtaining the maximal response from all applied agents and then dividing the measured change in I_{SC} by the maximal response to obtain a percent value. Data was transformed into a percent due to variability in baseline measurements between mounted tissues. Percent inhibition was calculated as follows:

Maximal response: $X_{\text{baseline Isc}}$-$Y_{\text{remaining Isc}}$

Percent Inhibition: $\frac{(X_{\text{Isc prior to drug application}} - Y_{\text{steady-state Isc after drug application}})}{\text{Maximal response}}$

Dose-Response. This was performed to calculate a half-maximal inhibitory concentration (IC_{50}) for flupirtine (general Kv7 agonist) and ICA 110381 (specific agonist of Kv7.2/3). Pharmacological agents were diluted from their respective stock concentrations to a range of 10^{-4} M to 10^{-1} M, which were then diluted 1:1000 (5 µL into 5 mL) within the chamber. Different concentrations were added sequentially, starting with 10^{-4} M and increasing by a factor of 10 for each addition. Tissue was allowed to reach a steady-state prior to the application of the next administered dose.

Statistics. All presented data represent mean ± standard error (sem) from five different animals, unless otherwise denoted within the text. Statistical tests that were performed on the presented data was student's unpaired t-test using Graphpad Prism 5.0 (San Diego, CA). $p < 0.001$ was used for the determination of significance.

Stock solutions. Indomethacin was prepared as a 5 mM stock solution in ethanol. Ussing chamber stocks are as follows: 1 mM tetrodotoxin (TTX, dissolved in acetic acid, Tocris Pharmaceuticals, Minneapolis, MN), 10 mM tolterodine (TOL, dissolved in H_2O, Tocris Pharmaceuticals, Minneapolis, MN), 50 mM flupirtine (FLU, dissolved in DMSO, Tocris Pharmaceuticals, Minneapolis,

MN), 50 mM ICA 110381 (ICA, dissolved in DMSO, Tocris Pharmaceuticals, Minneapolis, MN), 50 mM nicotine (NICO, dissolved in H_2O, Tocris Pharmaceuticals, Minneapolis, MN), 10 mM forskolin (FSK, dissolved in DMSO, Tocris Pharmaceuticals, Minneapolis, MN), and 50 mM XE-991 (dissolved in H_2O, Tocris Pharmaceuticals, Minneapolis, MN).

Results

Inhibition of I_{SC} in Whole-Mount Colon with the Kv7 Activator Flupirtine. Previous studies have shown that inhibition of the ENS with tetrodotoxin (TTX), a voltage-sensitive Na^+ channel (Na_V) inhibitor, was able to significantly attenuate the on-going basal Cl^- secretion in Ussing chambers [25]. This is accomplished via inhibiting propagation of action potentials and eventual release of neurotransmitters [26]. With this in mind, flupirtine, a Kv7 activator that hyperpolarizes neurons and ultimately decreases release of neurotransmitter, could be applied to indirectly inhibit on-going Cl^- secretion. As demonstrated by the representative trace (Fig. 1A), basolateral 100 μM flupirtine application was able to significantly decrease the observed I_{SC} from the mounted tissue. However, basolateral application of 1 μM TTX only slightly decreased I_{SC} (Fig. 1A). Group data of 100 μM flupirtine application prior to 1 μM TTX administration demonstrated a similar pattern of flupirtine being responsible for a significant majority of the percent of inhibited I_{SC} (FLU vs. TTX, 94.23 ± 1.50 % vs. 5.77 ± 1.50 %) (Fig. 1C). However, administration of 1 μM TTX prior to flupirtine resulted in a significant decrease in measured I_{SC}, while flupirtine only slightly decreased

I_{SC} (Fig. 1B). Group data of TTX administration prior to flupirtine also demonstrated a similar pattern with TTX conferring a majority of the percent-inhibited I_{SC} in Ussing chamber experiments (TTX vs. FLU, 77.92 ± 6.6 % vs. 22.08 ± 6.6 %, p< 0.001) (Fig.1D). Comparison of order of administration demonstrated flupirtine following TTX application was significantly less than when administered prior to TTX (22.08 ± 6.58 % vs. 94.23 ± 1.50 %, Fig. 1E).

Dose-Response of I_{SC} to Basolateral Flupirtine Application. Following the initial finding of flupirtine decreasing I_{SC} in colonic epithelium, we decided to more fully characterize the drug by determining a half-maximal inhibitory concentration (IC_{50}). Initial administration of 100 nM flupirtine was unable to elicit any effect on the tissue, as demonstrated by the representative trace (Fig. 2A). However, increasing doses of flupirtine, from 1 μM up to highest concentration of 100 μM, were able to inhibit the on-going I_{SC} (Fig. 2A). The data as a whole demonstrated a significant inhibition with the addition of 10 μM flupirtine, which accounted for a 49.44 ± 5.9 % decrease from the previous baseline current. 100 μM flupirtine application was also able to further decrease I_{SC} (37.48 ± 3.8 %), however not as robustly as the previously administered 10 μM dose, which would indicate reaching an asymptote of effect (Fig. 2B). Utilizing a non-linear fit to the calculated percent of inhibition presented in Fig. 2B, we were able to calculate an IC_{50} for flupirtine of 9.37 ± 0.42 μM.

Inhibition of on-going I_{SC} in Colonic Epithelium with the Muscarinic Antagonist Tolterodine. As described previously, Na_V channels are located within ENS neurons, so inhibition of those channels with TTX would inhibit neurotransmitter release (i.e. acetylcholine) onto epithelial cells. To further establish that basolateral flupirtine may be acting on ENS neurons, we decided to use the muscarinic antagonist tolterodine to inhibit acetylcholine activation of muscarinic receptors on epithelial cells. As expected and in concordance with literature [27], basolateral application of 10 μM tolterodine was able to inhibit a significant amount of basal I_{SC} (80.35 ± 3.72 %, Fig. 3C), as illustrated by the representative trace (Fig. 3A). Addition of 100 μM flupirtine was able to further decrease I_{SC} (19.65 ± 3.72 %, Fig. 3A/C). However, the addition of 100 μM flupirtine prior to 10 μM tolterodine application demonstrated a significant inhibition of I_{SC} (99.59 ± 0.41 %, Fig. 3B/D), more similar to flupirtine administration prior to 1 μM TTX (Fig. 1D). Unexpectedly though, addition of 10 μM tolterodine to the basolateral surface led to a paradoxical increase in I_{SC} (-15.2 ± 8.56 % Fig. 3B/D), as opposed to the decrease in I_{SC} observed with flupirtine application. Comparison of order of administration demonstrated that flupirtine administration prior to tolterodine resulted in a significant increase in percent of inhibition (99.59 ± 0.41 % vs. 19.65 ± 3.72 %, Fig. 3E).

Pre-Incubation with Flupirtine Inhibits Basolaterally-Administered Nicotine-Induced I_{SC}. Increased firing of ENS neurons has previously been shown to elicit increases in measured I_{SC} [4]. In line with this notion, we decided to activate ENS

neurons via basolateral addition of 100 μM nicotine. As illustrated by the representative trace (Fig. 4A), basolateral administration of nicotine dramatically increased measured I_{SC}. Tissue that was pre-incubated with 100 μM flupirtine did exhibit the expected decrease in I_{SC}. However, addition of 100 μM nicotine was not able to stimulate I_{SC} (Fig. 4B). Tissues that received nicotine-only were able to elicit large increases in I_{SC}, while tissues that were pre-incubated with flupirtine were practically unresponsive to nicotine (93.22 ± 18.86 μA/cm^2 vs. 0.26 ± 1.12 μA/cm^2, Fig. 4C).

Application of Flupirtine and TTX in T_{84} Monolayers Does Not Inhibit I_{SC}.

T_{84} monolayers have been used to study the colonic epithelium for several decades [28, 29]. The T_{84} cell line was originally isolated from a colonic adenocarcinoma**,** and consists of a homogenous population of secretory epithelium [30]. Therefore, application of any pharmacological agents that interact with ENS neurons to exert their effect would not demonstrate an efficacy in the T_{84} cell line. To establish this within our lab, we first mounted T_{84} monolayers in the Ussing chamber, and upon reaching a steady-state applied 1 μM TTX to the basolateral surface of the monolayer. TTX was without effect (Fig. 5A/C), however to confirm that monolayers were functioning as a tight epithelium 10 μM forskolin (FSK) was applied basolaterally. As expected, 10 μM FSK was able to increase I_{SC} dramatically (24.58 ± 2.88 μA/cm^2, Fig. 5A/D). Following this outcome, another group of monolayers were administered 100 μM flupirtine to the basolateral side of the chamber. As previously seen with TTX application,

100 μM flupirtine was unable to decrease measured I_{SC}, however, there was a very modest increase in baseline I_{SC} (0.57 ± 0.23 μA/cm^2, Fig. 5B/C). T_{84} monolayers were once again administered 10 μM FSK, which significantly increased I_{SC} (24.61 ± 4.21 μA/cm^2) to comparable levels of T_{84} monolayers exposed to TTX (Fig. 5D). Both groups were then exposed to 50 μM XE-991 (Kv7 antagonist), which demonstrated a significant inhibition of of FSK-stimulated I_{SC} (Fig. 5A/B)

Kv7.2 and K_V7.3 Exhibit Co-Localization with Choline Acetyl Transferase in ENS Neurons. Since previous work has shown that K_V7.2/3 are crucial to the native M current in neurons and may contribute to the observed effect of flupirtine on I_{SC}, we decided to immuno-label for the two different channels in whole mount tissue. Choline acetyl transferase (ChAT) was used as a marker of enteric neurons due to the high abundance of cholinergic neurons in the ENS, and potential co-localization of the ion channels of interest. ChAT consistently labeled axons of enteric neurons, as illustrated by Fig. 6A/D. K_V7.2 and K_V7.3 (Fig. 6B/E) consistently co-localized with enteric neuronal axons that were positively immuno-stained for ChAT (Fig. 6C/F).

ICA 110381, **a Specific Activator of K_V7.2/3, Inhibits I_{SC} in a Dose-Dependent Manner.** Following identification of K_V7.2 and K_V7.3 in ENS neurons, we decided to use a specific activator of the heterotetramer, K_V7.2/3. ICA 110381 has previously demonstrated selectivity for K_V7.2/3 over the other members of the

KCNQ family of K^+ channels [31]. Basolateral application of 100 μM ICA was able to significantly inhibit the I_{SC} (Fig. 7A). Similar to before with flupirtine, administration of 1 μM TTX following ICA was practically unable to decrease I_{SC} (Fig. 7A). ICA 110381 was able to account for 96.88 ± 0.94 % of the total inhibited I_{SC}, while 1 μM TTX only inhibited 3.12 ± 0.94 % of the current (Fig. 7B). A dose-response curve was also generated for ICA 110381 (Fig. 7C). Concentrations ranging from 1 μM to 100 μM were able to decrease I_{SC}. The use of a non-linear fit of the grouped data allowed for the calculation of an IC_{50} for ICA 110381, which was 10.55 ± 0.75 μM (Fig. 7D).

Discussion

Our findings in this study indicate that hyperpolarization of enteric neurons with the K_V7 activator flupirtine is able to decrease resultant mucosal secretion via decreased neuronal firing. This conclusion is evidenced by the fact that flupirtine administration prior to TTX leads to substantial inhibition of baseline I_{SC}, however the simple reversal of that order leads to a significant inhibition of I_{SC} by TTX with a much smaller contribution from flupirtine (Fig. 1). As not to rely on this as our only evidence, we then characterized the ability of flupirtine to inhibit nicotine-stimulated I_{SC}, which is mediated through nicotinic receptors on post-ganglionic fibers [32]. Control tissue administered basolateral nicotine demonstrated a significant increase in I_{SC}, however pre-incubation with flupirtine left the tissue practically unresponsive, owing to ENS neurons being substantially hyperpolarized (Fig. 4). Also, to more fully implicate the ENS in mediating the

effects of flupirtine, T_{84} monolayers [30] did not exhibit a decrease in I_{SC} upon basolateral administration (Fig. 5). We then wanted to try and characterize the specific K_V7 channels responsible for mediating the effects of flupirtine. Immunofluorescence studies demonstrated that the canonical M current channels, $K_V7.2$ and $K_V7.3$, co-localized with axons that stained positively for ChAT (Fig. 6). Finally, the use of the $K_V7.2/3$ activator, ICA 110381, demonstrated a similar profile to flupirtine administration (Fig. 7). In total, our results would indicate that the decrease in I_{SC} from basolateral application of flupirtine is ENS-mediated via hyperpolarization of enteric neurons through activation of $K_V7.2/3$.

$K_V7.1$, another member of the K_V7 family, has been localized and functionally described in epithelial tissues [33-35] and could be thought to participate in the observed response in native tissue. However, activation of $K_V7.1$ in epithelial tissues leads to an increase in K^+ recycling via the basolateral membrane and an increase in apical Cl^- secretion [36]. These previous observations would agree with our results that flupirtine was not able to decrease I_{SC} in T_{84} monolayers, but actually resulted in a small increase in I_{SC} [37] from activation of presumably of $K_V7.1$ (Fig. 5). To further demonstrate the importance of K_V7 in apical Cl^- secretion, XE-991, a non-specific K_V7 inhibitor, was administered to the basolateral membrane of T_{84} monolayers, which demonstrated a significant decrease in FSK-mediated I_{SC}.

The effect of flupirtine on cholinergic neurons was also studied, since cholinergic fibers make up approximately 60% of neurons within the ENS [38]. As

expected, tolterodine (muscarinic receptor antagonist) application was able to partially inhibit on-going mucosal Cl^- secretion [39, 40]. Flupirtine was able to further decrease measured I_{SC}. This would indicate that non-cholinergic neurotransmitters also participate in modulating mucosal electrolyte transport, which has also been previously described [25]. Application of flupirtine prior to tolterodine would then be expected to inhibit all ENS neurons, and the application of the muscarinic receptor antagonist following this would have no effect or only very modestly decrease I_{SC}. However, tolterodine application following flupirtine administration unexpectedly increased I_{SC} (Fig. 3B/D). This could be the result of a subpopulation of interneurons that are less sensitive to flupirtine. Application of tolterodine would block the remaining excitatory stimulation on inhibitory secretomotor neurons, which would remove the “brake”, and lead to the observed increase in I_{SC}.

Previous studies have shown that several gastrointestinal disorders result in an overall increase in excitability of ENS neurons [8-10, 41]. However, current clinical options are limited for these pathologies, with many observed adverse effects [42, 43]. Unfortunately, flupirtine, which had been available for nearly three decades in several European countries, was recently removed from the market due to issues of hepatotoxicity [44]. Development of novel K_V7 channel activators, with a greater safety profile, could yield therapeutic potential in patients that have been unresponsive to traditional treatments for an over-active ENS. Since K_V7 channel activation causes a sustained hyperpolarization of enteric neurons that synapse on the epithelium, as well as the smooth muscle,

targeted treatment could help to alleviate associated-symptoms. Also, our immunofluorescence studies demonstrate localization of $K_V7.3$ in gastrointestinal smooth muscle (Fig. 6), which along with previous observations of K_V7 channels in smooth muscle may further enhance the efficacy of a K_V7 activator by reducing motility of gastrointestinal tract [45]. In all, K_V7 activators could potentially be utilized clinically for the treatment of gastrointestinal disorders attributed to hyper-excitability of the ENS.

In summary, our results demonstrate that activation of K_V7 channels via flupirtine in enteric neurons significantly inhibits mucosal electrolyte transport in the colon. As demonstrated through immunofluorescence studies and a specific pharmacological activator, this mechanism is mediated through $K_V7.2/3$ located within axons of enteric neurons. Also, this discovery may have clinical significance as a potential therapeutic agent to decrease ENS hyper-excitability in certain gastrointestinal pathologies and associated-outcomes.

References

1. Furness, J.B., *The enteric nervous system and neurogastroenterology.* Nat Rev Gastroenterol Hepatol, 2012. **9**(5): p. 286-94.
2. Costa, M. and J.B. Furness, *The origins, pathways and terminations of neurons with VIP-like immunoreactivity in the guinea-pig small intestine.* Neuroscience, 1983. **8**(4): p. 665-76.
3. Riegler, M., et al., *Neurotensin stimulates Cl(-) secretion in human colonic mucosa In vitro: role of adenosine.* Gastroenterology, 2000. **119**(2): p. 348-57.
4. Schulzke, J.D., et al., *Ion transport and enteric nervous system (ENS) in rat rectal colon: Mechanical stretch causes electrogenic Cl-secretion via Plexus Meissner and amiloride-sensitive electrogenic Na-absorption is not affected by intramural neurons.* Pflügers Archiv European Journal of Physiology, 1989. **414**(2): p. 216-221.
5. Szurszewski, J.H., *A migrating electric complex of canine small intestine.* Am J Physiol, 1969. **217**(6): p. 1757-63.
6. Kenny, S.E., P.K. Tam, and M. Garcia-Barcelo, *Hirschsprung's disease.* Semin Pediatr Surg, 2010. **19**(3): p. 194-200.
7. Lakhan, S.E. and A. Kirchgessner, *Neuroinflammation in inflammatory bowel disease.* J Neuroinflammation, 2010. **7**: p. 37.
8. Lundgren, O., et al., *Role of the enteric nervous system in the fluid and electrolyte secretion of rotavirus diarrhea.* Science, 2000. **287**(5452): p. 491-5.

9. Houghton, L.A., J.M. Foster, and P.J. Whorwell, *Alosetron, a 5-HT3 receptor antagonist, delays colonic transit in patients with irritable bowel syndrome and healthy volunteers.* Aliment Pharmacol Ther, 2000. **14**(6): p. 775-82.

10. Linden, D.R., K.A. Sharkey, and G.M. Mawe, *Enhanced excitability of myenteric AH neurones in the inflamed guinea-pig distal colon.* J Physiol, 2003. **547**(Pt 2): p. 589-601.

11. Koussoulas, K., et al., *Cholera toxin induces sustained hyperexcitability in myenteric, but not submucosal, AH neurons in guinea pig jejunum.* Gastroenterology, 2017. **136**(1): p. 299-308 e4.

12. Franks, C.J., et al., *Ionic basis of the resting membrane potential and action potential in the pharyngeal muscle of Caenorhabditis elegans.* J Neurophysiol, 2002. **87**(2): p. 954-61.

13. Ng, F.L., et al., *Expression and function of the K+ channel KCNQ genes in human arteries.* Br J Pharmacol, 2011. **162**(1): p. 42-53.

14. Shah, M.M., et al., *Functional significance of axonal Kv7 channels in hippocampal pyramidal neurons.* Proc Natl Acad Sci U S A, 2008. **105**(22): p. 7869-74.

15. Anderson, U.A., C. Carson, and K.D. McCloskey, *KCNQ currents and their contribution to resting membrane potential and the excitability of interstitial cells of Cajal from the guinea pig bladder.* J Urol, 2009. **182**(1): p. 330-6.

16. Brown, D.A. and G.M. Passmore, *Neural KCNQ (Kv7) channels.* Br J Pharmacol, 2009. **156**(8): p. 1185-95.

17. Wang, Z.P., Wenmei Shi, Barry S. Brown,Randy S. Wymore, Ira S. Cohen, Jane E. Dixon,* David McKinnon, *KCNQ2 and KCNQ3 Potassium Channel Subunits: Molecular Correlates of the M-Channel.* Science, 1998. **282**(5395): p. 1890-1893.

18. King, C.H., et al., *Kv7.2 regulates the function of peripheral sensory neurons.* J Comp Neurol, 2014. **522**(14): p. 3262-80.

19. Peters, H.C., et al., *Conditional transgenic suppression of M channels in mouse brain reveals functions in neuronal excitability, resonance and behavior.* Nat Neurosci, 2005. **8**(1): p. 51-60.

20. Roche, J.P., et al., *Antibodies and a cysteine-modifying reagent show correspondence of M current in neurons to KCNQ2 and KCNQ3 K + channels.* British Journal of Pharmacology, 2002. **137**(8): p. 1173-1186.

21. Bi, Y., et al., *Visceral hyperalgesia induced by forebrain-specific suppression of native Kv7/KCNQ/M-current in mice.* Mol Pain, 2011. **7**: p. 84.

22. Watanabe, H., et al., *Disruption of the epilepsy KCNQ2 gene results in neural hyperexcitability.* J Neurochem, 2000. **75**(1): p. 28-33.

23. Peiris, M., et al., *Peripheral KV7 channels regulate visceral sensory function in mouse and human colon.* Mol Pain, 2017. **13**: p. 1744806917709371.

24. Rottgen, T.S., et al., *Dextran Sulfate Sodium (DSS)-induced Chronic Colitis Attenuates Ca(2+)-activated Cl(-) Secretion in Murine Colon by Down-regulating TMEM16A.* Am J Physiol Cell Physiol, 2018.

25. Belai, A., J. Lincoln, and G. Burnstock, *Lack of release of vasoactive intestinal polypeptide and calcitonin gene-related peptide during electrical stimulation of enteric nerves in streptozotocin-diabetic rats.* Gastroenterology, 1987. **93**(5): p. 1034-40.

26. Kostyuk, P.G., N.S. Veselovsky, and A.Y. Tsyndrenko, *Ionic currents in the somatic membrane of rat dorsal root ganglion neurons-I. Sodium currents.* Neuroscience, 1981. **6**(12): p. 2423-30.

27. Kuwahara, A. and H.J. Radowicz-Cooke, *Epithelial transport in guinea-pig proximal colon: influence of enteric neurones.* J Physiol, 1988. **395**: p. 271-84.

28. Stutts, M.J., et al., *Activation of CFTR Cl- conductance in polarized T84 cells by luminal extracellular ATP.* Am J Physiol, 1995. **268**(2 Pt 1): p. C425-33.

29. Sun, H., et al., *Tgf-beta downregulation of distinct chloride channels in cystic fibrosis-affected epithelia.* PLoS One, 2014. **9**(9): p. e106842.

30. Dharmsathaphorn, K., et al., *A human colonic tumor cell line that maintains vectorial electrolyte transport.* Am J Physiol, 1984. **246**(2 Pt 1): p. G204-8.

31. Boehlen, A., et al., *The new KCNQ2 activator 4-Chlor-N-(6-chlor-pyridin-3-yl)-benzamid displays anticonvulsant potential.* Br J Pharmacol, 2013. **168**(5): p. 1182-200.

32. Sheldon, R.J., et al., *Pharmacological characterization of neural mechanisms regulating mucosal ion transport in mouse jejunum.* J Pharmacol Exp Ther, 1989. **249**(2): p. 572-82.

33. Kunzelmann, K., et al., *Cloning and function of the rat colonic epithelial K+ channel KVLQT1.* J Membr Biol, 2001. **179**(2): p. 155-64.

34. MacVinish, L.J., et al., *Importance of basolateral K+ conductance in maintaining Cl- secretion in murine nasal and colonic epithelia.* J Physiol, 1998. **510 (Pt 1)**: p. 237-47.

35. Mall, M., et al., *Role of K(V)LQT1 in cyclic adenosine monophosphate-mediated Cl(-) secretion in human airway epithelia.* Am J Respir Cell Mol Biol, 2000. **23**(3): p. 283-9.

36. Grahammer, F., et al., *The small conductance K+ channel, KCNQ1: expression, function, and subunit composition in murine trachea.* J Biol Chem, 2001. **276**(45): p. 42268-75.

37. Schroeder, B.C., et al., *A constitutively open potassium channel formed by KCNQ1 and KCNE3.* Nature, 2000. **403**(6766): p. 196-9.

38. Qu, Z.D., et al., *Immunohistochemical analysis of neuron types in the mouse small intestine.* Cell Tissue Res, 2008. **334**(2): p. 147-61.

39. Chandan, R., et al., *Cholinergic neurons and muscarinic receptors regulate anion secretion in pig distal jejunum.* Eur J Pharmacol, 1991. **193**(3): p. 265-73.

40. Chandan, R., et al., *Muscarinic cholinergic regulation of electrogenic chloride secretion in porcine proximal jejunum.* J Pharmacol Exp Ther, 1991. **257**(2): p. 908-17.

41. Palmer, J., Wong-Riley Margaret, Sharkey Keith, *Functional alterations in jejunal myenteric neurons during inflammation in nematode-infected guinea pigs.* American Journal of Physiology, 1998. **275**(38): p. 922-935.

42. Gallo-Torres, H., A. Brinker, and M. Avigan, *Alosetron: ischemic colitis and serious complications of constipation.* Am J Gastroenterol, 2006. **101**(5): p. 1080-3.

43. Page, J.G. and G.M. Dirnberger, *Treatment of the irritable bowel syndrome with Bentyl (dicyclomine hydrochloride).* J Clin Gastroenterol, 1981. **3**(2): p. 153-6.

44. Michel, M.C., et al., *Unexpected frequent hepatotoxicity of a prescription drug, flupirtine, marketed for about 30 years.* Br J Clin Pharmacol, 2012. **73**(5): p. 821-5.

45. Jepps, T.A., et al., *Molecular and functional characterization of Kv7 K+ channel in murine gastrointestinal smooth muscles.* Am J Physiol Gastrointest Liver Physiol, 2009. **297**(1): p. G107-15.

Figure Legends

Figure 1. **Basolateral 100 μM Flupirtine Inhibits I_{SC} in the Murine Distal Colon.** *A.* Representative trace of basolateral application of 1 μM tetrodotoxin

(TTX) on full thickness tissue preparation in the Ussing chamber. TTX was able to decrease I_{SC}, however addition of basolateral 100 μM flupirtine (Flu) following the TTX-induced plateau only modestly decreased I_{SC}. *B.* Representative trace of basolateral application of 100 μM Flu in the Ussing chamber. Measured I_{SC} substantially decreased from the previous baseline, however application of 1 μM TTX only slightly decreased measured I_{SC}. *C*. Group data of percent inhibition of maximal response of 1 μM TTX prior to 100 μM Flu. *D.* Group data of percent inhibition of maximal response of 100 μM Flu prior to 1 μM TTX application. *E.* Group data of percent inhibition of maximal response of 100 μM Flu prior to or following TTX application. All presented bar graphs are summarized data of means ± SE from five different animals (n=5). Plotted points on each bar graph are representative of individual experiments. *$p < 0.001$ – compared to control.

Figure 2. **Dose-Response of Basolateral application of Flupirtine in Murine Distal Colon.** *A.* Representative trace of a dose-response curve of Flu. The initial administered concentration of Flu was 100 nM and increased sequentially by a log order of 10 until reaching a final concentration of 100 μM Flu. Each arrow within the trace indicates time of administration of an individual dose of Flu. *B.* A dose-response curve of percent inhibition of maximal response was generated from multiple experiments (n=5) to determine an approximate half-maximal inhibitory concentration (IC_{50}) in the murine distal colon.

Figure 3. **Tolterodine and Flupirtine Inhibit Cholinergic-induced I_{SC} in the Distal Colon.** *A.* Representative trace of basolateral application of 10 μM tolterodine (TOL) followed by basolateral 100 μM Flu on whole-mount distal colon in the Ussing chamber. *B.* Representative trace of basolateral application of 100 μM Flu followed by 10 μM TOL in the Ussing chamber. *C.* Group data of percent inhibition of maximal response of 10 μM TOL prior to Flu application. *D*. Group data of percent inhibition of maximal response of 100 μM Flu prior to application 10 μM TOL. *E.* Group data of percent inhibition of maximal response of 100 μM Flu prior to or following 10 μM TOL application. All presented bar graphs represent summarized data of means ± SE from five different animals (n=5). Plotted points on each bar graph represent individual experiments that contribute to the overall mean and SE. *$p < 0.001$

Figure 4. **Flupirtine Inhibits Nicotine-Induced Increases in I_{SC}.**

A. Representative trace of basolateral 100 μM nicotine (NICO)-induced increases in measured I_{SC} in the distal colon. *B.* Representative trace of 100 μM NICO-induced increases in I_{SC} that was pre-incubated with 100 μM Flu. *C.* Group data of NICO-induced ΔI_{SC} in tissue that was pre-incubated with or without 100 μM Flu prior to basolateral 100 μM NICO administration. All presented bar graphs represent summarized data of means ± SE from five different animals (n=5). Plotted points on each bar graph represent individual experiments that contribute to the overall mean and SE. *$p < 0.001$

Figure 5. **Flupirtine Does Not Decrease I_{sc} in T_{84} Monolayers.** *A.* Representative trace of measured I_{SC} in T_{84} monolayers that were treated with basolateral 100 μM Flu. Monolayers were then stimulated with 10 μM forskolin (FSK) that was inhibited with 50 μM XE-991 upon reaching a steady-state. *B.* Representative trace of measured I_{SC} in T_{84} monolayers that were incubated with 1 μM TTX. Monolayers were then stimulated with 10 μM FSK and then inhibited with 50 μM XE-991. *C.* Group data of measured ΔI_{SC} following either 100 μM Flu or 1 μM TTX. *D.* Group data of 10 μM FSK-induced ΔI_{SC} from T_{84} monolayers incubated with Flu or TTX. All presented bar graphs represent summarized data of means ± SE from five different animals (n=5). Plotted points on each bar graph represent individual experiments that contribute to the overall mean and SE. *p < 0.001

Figure 6. **K_V7.2 and K_V7.3 Co-Localize with Choline Acetyl Transferase in Enteric Neurons of the Murine Distal Colon.** *A/D.* Axons of enteric neurons that stained positive for choline acetyl transferase (ChAT). *B/E.* Positive immuno-staining for K_V7.2 and K_V7.3 in murine distal colon. *C/F.* Merged images of panels A/B and D/E demonstrate co-localization of K_V7.2 and K_V7.3 with axons positively-stained for ChAT.

Figure 7. **The Specific K_V7.2/3 Activator, ICA 110381, Inhibits I_{SC} in the Murine Distal Colon.** *A.* Representative trace of measured I_{SC} that has been administered 100 μM ICA 110381(ICA) to the basolateral surface. This was then

followed by 1 μM TTX application, which was also applied to the basolateral surface. *B.* Group data of percent inhibition of maximal response of tissues that received basolateral 100 μM ICA prior to 1 μM TTX. *C.* Representative trace of a dose-response curve that was sequentially administered 100 nM ICA, increasing by a factor of ten each time, with a final basolateral concentration of 100 μM ICA. Each arrow indicates the time of administration of each corresponding concentration of ICA. *D.* A dose-response of percent inhibition of maximal response from multiple experiments (n=5) was generated to determine the IC_{50} of ICA. All presented bar graphs represent summarized data of means ± SE from five different animals (n=5). Plotted points on each bar graph represent individual experiments that contribute to the overall mean and SE.

Figure 1.

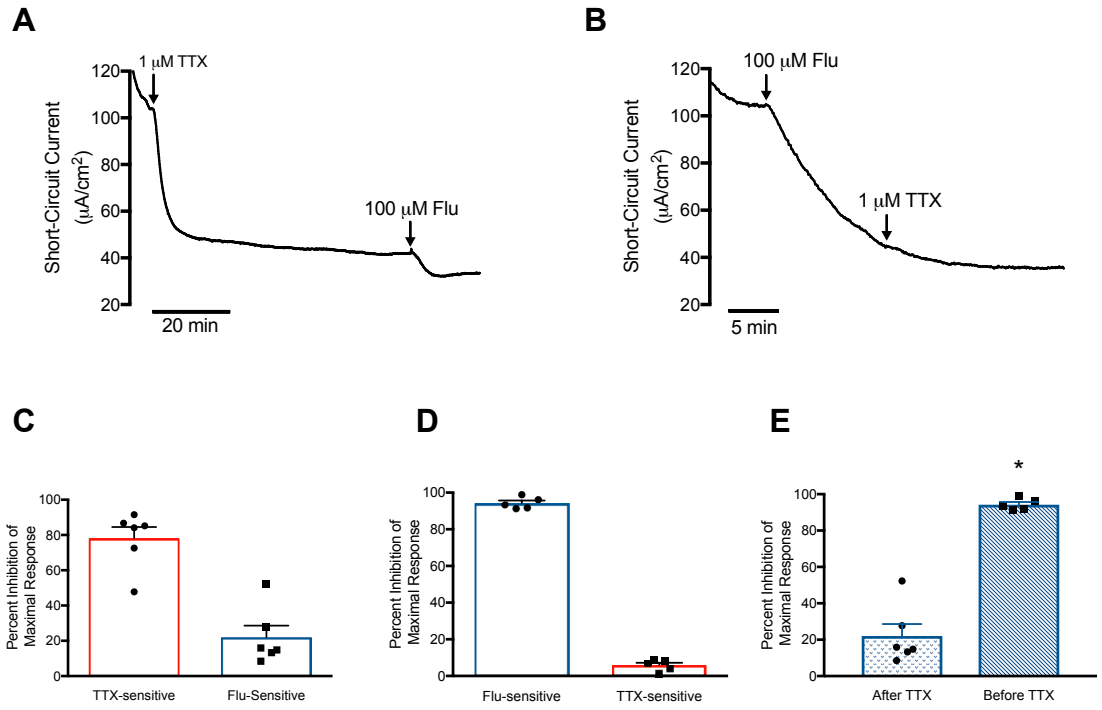
A
1 μM TTX
100 μM Flu
Short-Circuit Current (μA/cm²)
20 min
B
100 μM Flu
1 μM TTX
Short-Circuit Current (μA/cm²)
5 min
C
Percent Inhibition of Maximal Response
TTX-sensitive
Flu-Sensitive
D
Percent Inhibition of Maximal Response
Flu-sensitive
TTX-sensitive
E
*
Percent Inhibition of Maximal Response
After TTX
Before TTX

Figure 2.

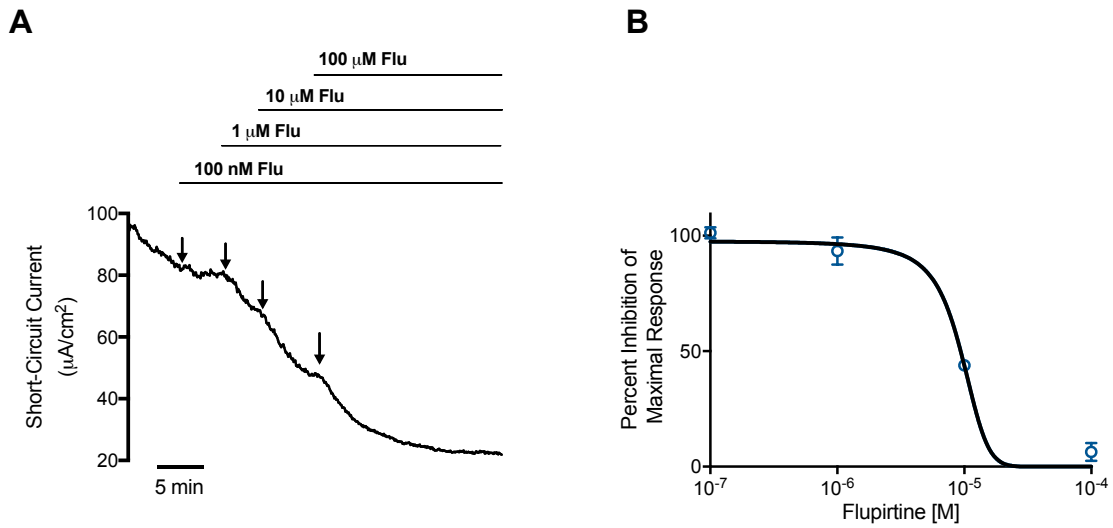
A
100 μM Flu
10 μM Flu
1 μM Flu
100 nM Flu
Short-Circuit Current (μA/cm²)
100
80
60
40
20
5 min
B
Percent Inhibition of Maximal Response
100
50
0
10⁻⁷
10⁻⁶
10⁻⁵
10⁻⁴
Flupirtine [M]

Figure 3.

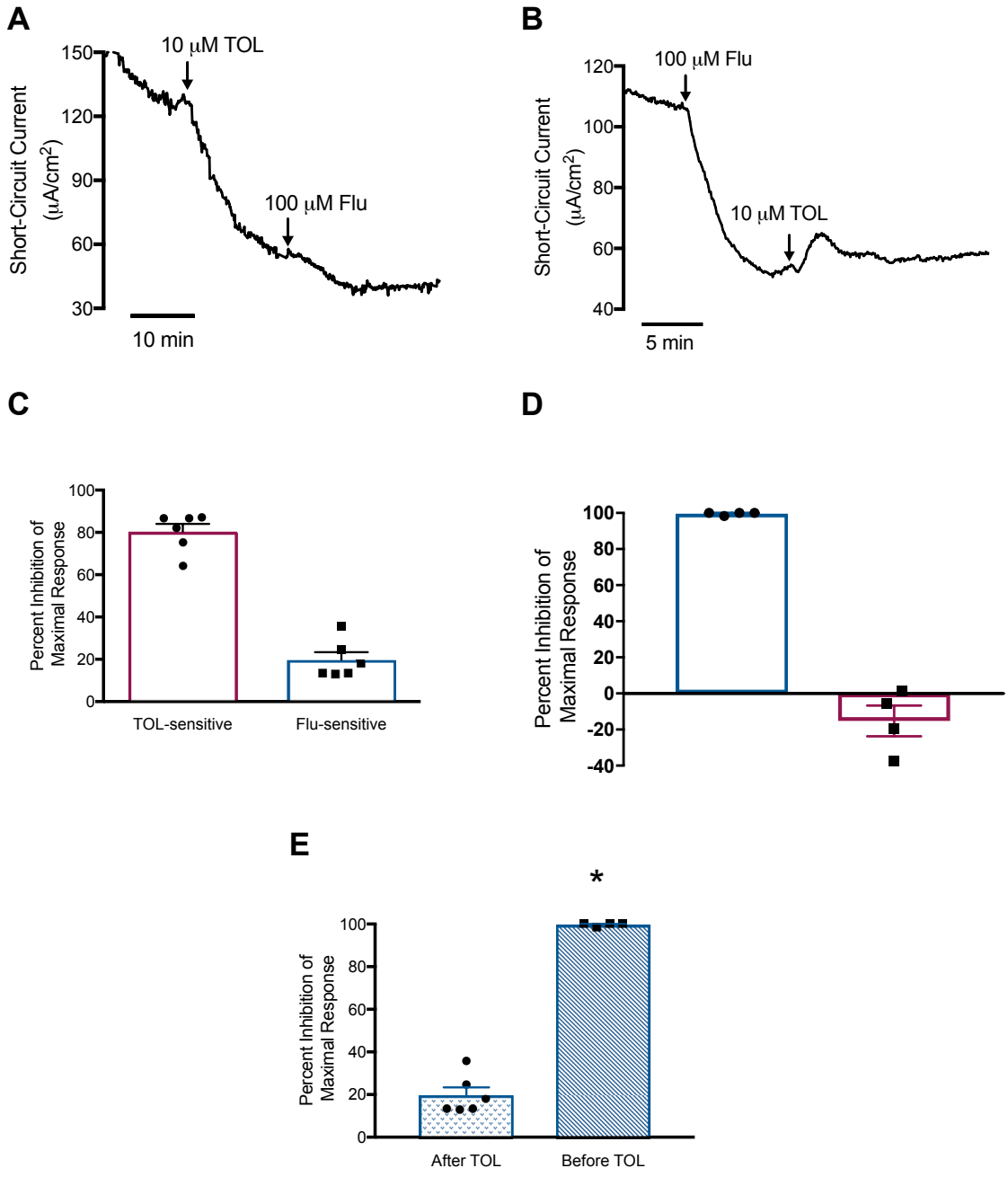
A
10 μM TOL
100 μM Flu
Short-Circuit Current (μA/cm²)
150
120
90
60
30
10 min
B
100 μM Flu
10 μM TOL
Short-Circuit Current (μA/cm²)
120
100
80
60
40
5 min
C
Percent Inhibition of Maximal Response
100
80
60
40
20
0
TOL-sensitive
Flu-sensitive
D
Percent Inhibition of Maximal Response
100
80
60
40
20
0
-20
-40
E
*
Percent Inhibition of Maximal Response
100
80
60
40
20
0
After TOL
Before TOL

Figure 4.

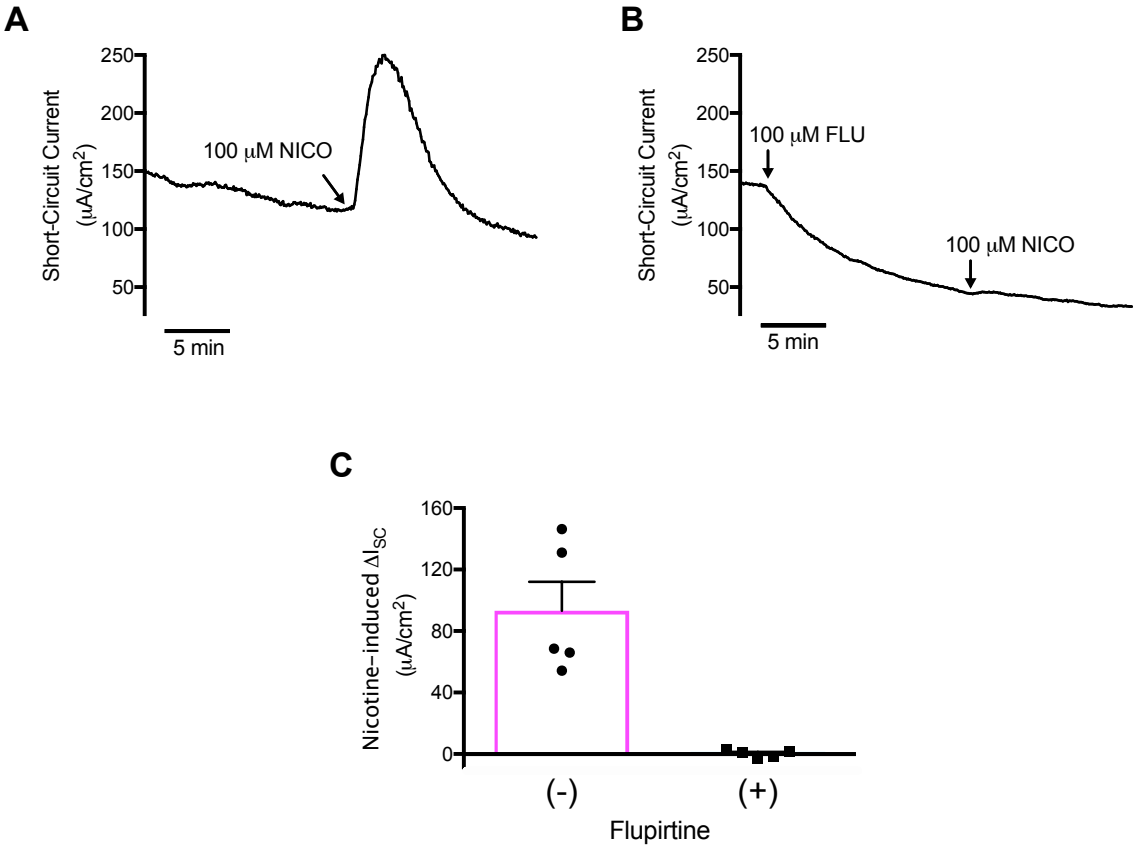
A
250
200
150
100
50
Short-Circuit Current
(μA/cm²)
100 μM NICO
5 min
B
250
200
150
100
50
Short-Circuit Current
(μA/cm²)
100 μM FLU
100 μM NICO
5 min
C
160
120
80
40
0
Nicotine-induced ΔI_SC
(μA/cm²)
(-)
(+)
Flupirtine

Figure 5.

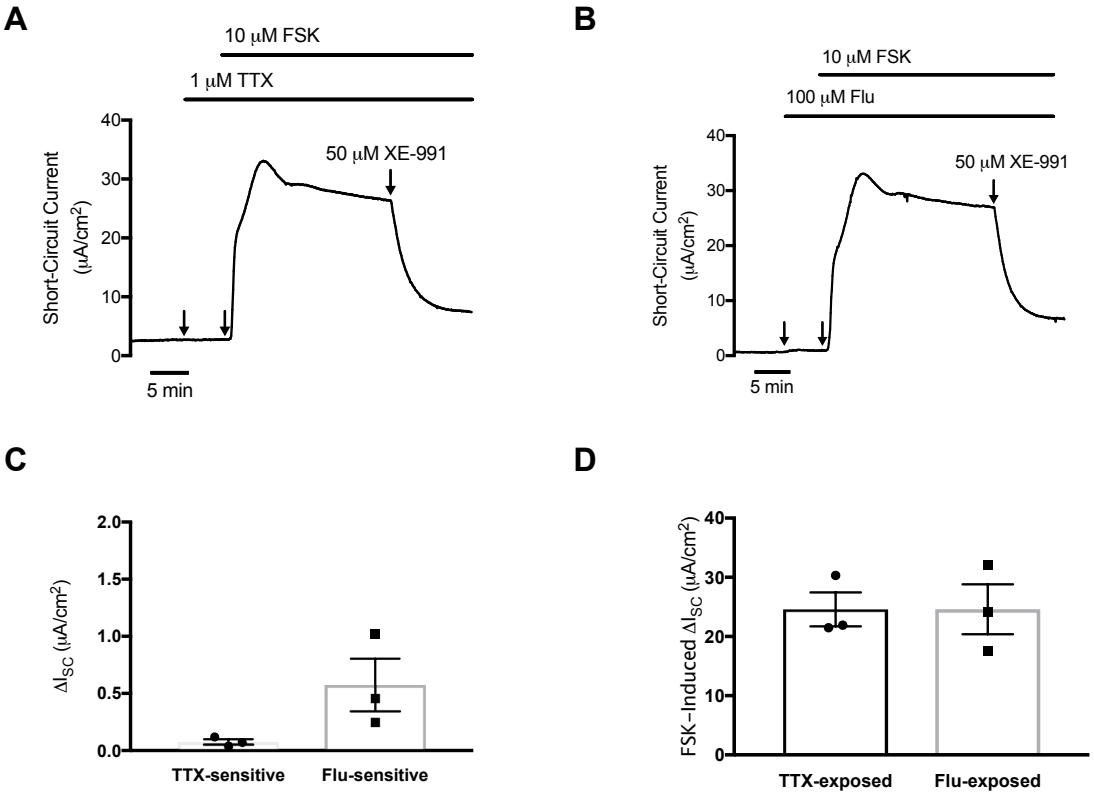
A
10 μM FSK
1 μM TTX
50 μM XE-991
Short-Circuit Current (μA/cm²)
5 min
B
10 μM FSK
100 μM Flu
50 μM XE-991
Short-Circuit Current (μA/cm²)
5 min
C
ΔISC (μA/cm²)
TTX-sensitive
Flu-sensitive
D
FSK–Induced ΔISC (μA/cm²)
TTX-exposed
Flu-exposed

Figure 6.

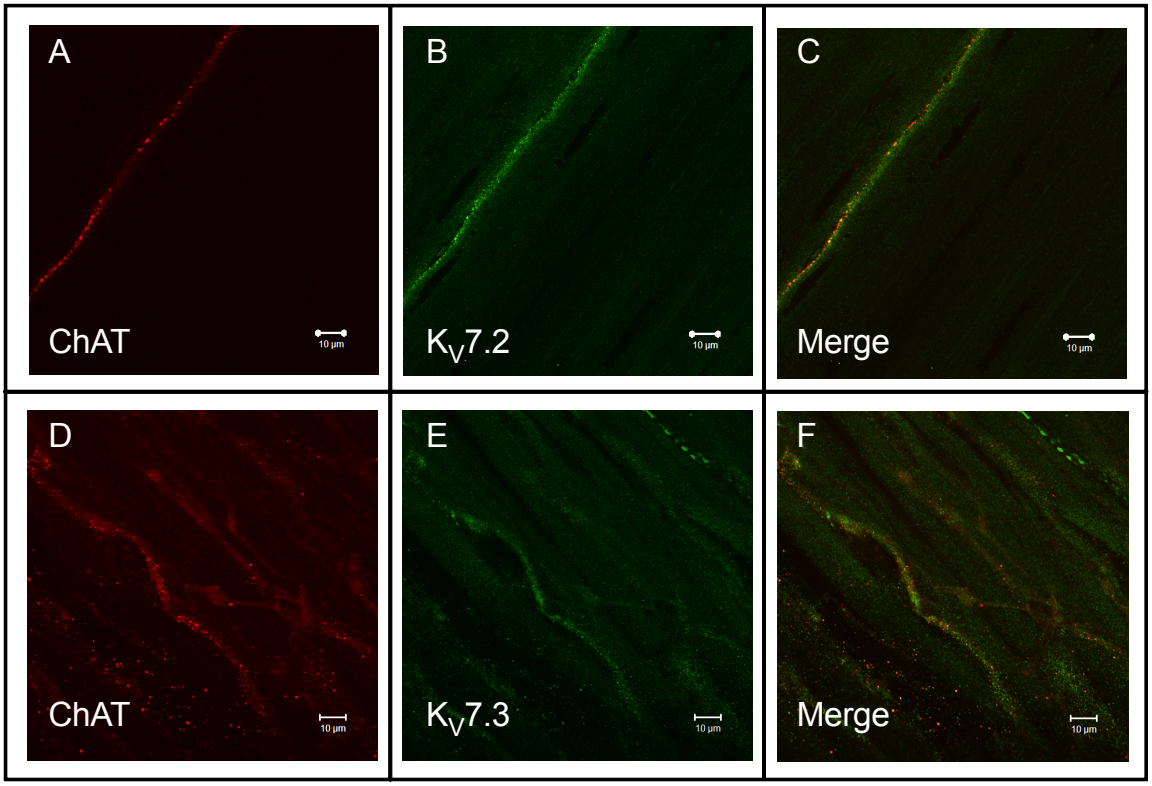
A
ChAT
10 µm
B
K_V7.2
10 µm
C
Merge
10 µm
D
ChAT
10 µm
E
K_V7.3
10 µm
F
Merge
10 µm

Figure 7.

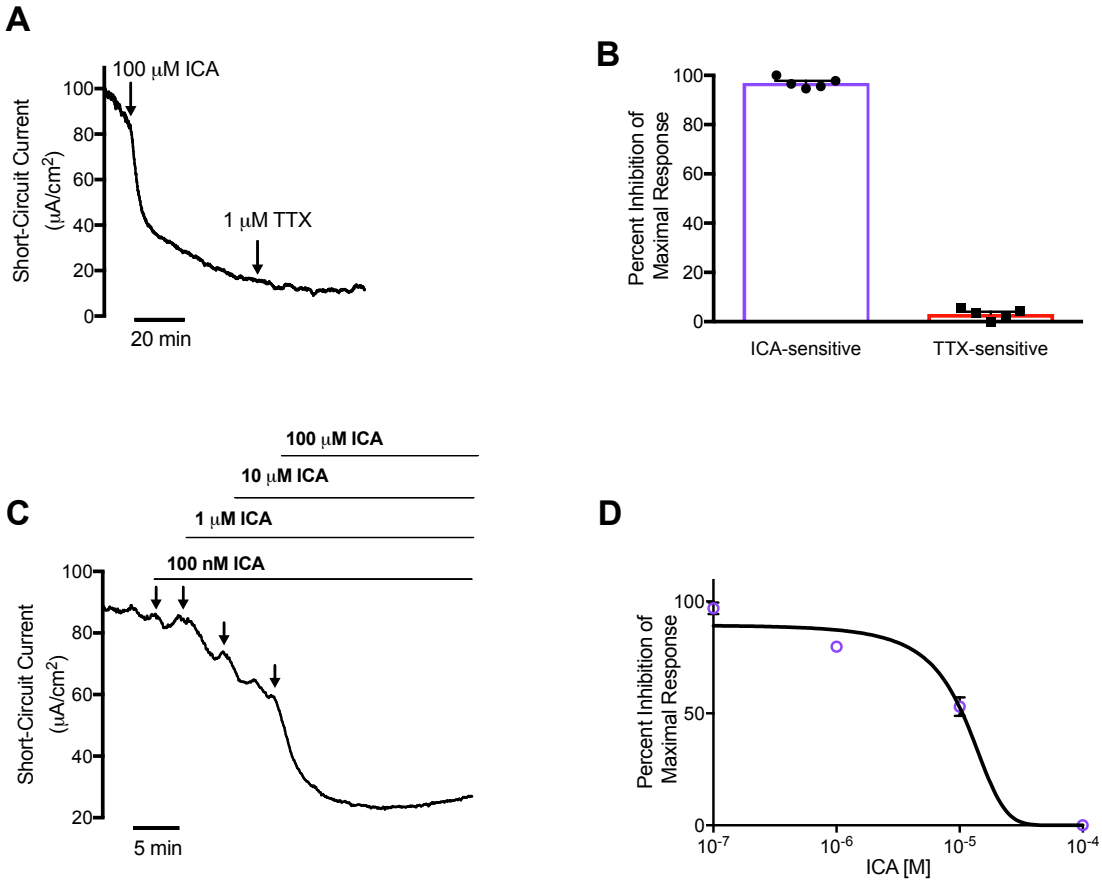
A
100 μM ICA
1 μM TTX
Short-Circuit Current (μA/cm²)
20 min
B
Percent Inhibition of Maximal Response
ICA-sensitive
TTX-sensitive
C
100 μM ICA
10 μM ICA
1 μM ICA
100 nM ICA
Short-Circuit Current (μA/cm²)
5 min
D
Percent Inhibition of Maximal Response
ICA [M]

Chapter IV

Conclusions and Proposal of Future Work

As previously presented, I have demonstrated that the absence of Ca^{2+}-activated Cl^- secretion in DSS-treated animals is a result of decreased expression of TMEM16A in colonic epithelium. I have also shown that activation of KCNQ2/3 and the resultant hyperpolarization in enteric neurons can inhibit mucosal Cl^- secretion. Each of these are novel findings and contribute to their respective fields. The following discussion will elaborate on their greater implications with a specific focus on inflammatory bowel disease.

TMEM16A and Dextran-Sulfate Sodium-Induced Colitis

As previously discussed, the DSS-induced colitis is a commonly utilized animal model of inflammatory bowel disease (IBD) [1]. It has previously been shown that the colitis that develops significantly blunts apical Cl^- secretion in the distal colon [2]. More specifically though, agonists that elicit increases in intracellular Ca^{2+} and resultant Cl^- secretion have been shown to be completely abolished. Stimulation with agonists that normally increase I_{SC} actually lead to a decrease following DSS treatment. Previous studies that focused on this phenomenon attributed these changes to a dysfunctioning ENS or alterations in the basolateral K^+ conductance [3, 4]. However, these studies were prior to the identification of TMEM16A, a CaCC. Our group was the first to reexamine this previously observed effect of DSS-induced colitis, and we were able to determine that TMEM16A was in fact down-regulated in the DSS-induced colitis model. Our functional data demonstrated that CCH-induced Cl^- secretion in DSS animals was not only abolished, but it had reversed in its direction of polarity, similar to previous reports. Also, the use of a Ca^{2+} ionophore (ionomycin) was able to

reproduce a similar I_{SC} profile to that of CCH, indicating this mechanism is mediated via Ca^{2+}. However, most important of all the findings was the quantification of TMEM16A via immunoblot. Immunoblot analysis demonstrated a significant reduction in total TMEM16A in colonic epithelium. Immunohistochemistry also demonstrated that the remaining protein was not properly trafficked to the cellular membrane in colonic epithelium.

While this seems to answer the question as to why Ca^{2+}-activated Cl^- secretion is absent in DSS-exposed animals, it does not solve the entire riddle. The mechanism by which TMEM16A is down-regulated in colonic epithelium following DSS-exposure is still unknown. However, several groups have previously demonstrated that Ca^{2+}-activated Cl^- secretion could be decreased following incubation with certain cytokines in immortalized cell lines of colonic epithelium [5, 6]. Both cytokines (IL-4 and TGF-β) that decreased Ca^{2+}-activated Cl^- secretion are more typically represented in a Th_2-mediated immune response. Since, the utilization of the Balb/c mice in our study typically respond in more of a Th_2 response (and our qPCR results would indicate as such), this may be the reason for loss of TMEM16A protein expression. With this as our working hypothesis, it would be interesting to repeat this study in C57Bl/6 mice, which typically demonstrate a Th_1 response upon DSS exposure, and determine if they would demonstrate a protection against loss of TMEM16A. Also, colon specific-knockout of TGF-β or IL-4 in combination with DSS-induction could potentially provide some protective mechanism by preventing signaling through either cellular pathway.

While signaling through a Th_2 immune response may be a likely cause for down-regulation of TMEM16A, the most important question to answer is, 'Does down-regulation of TMEM16A have any role in the development of or continuance of inflammation in DSS-colitis, or for that matter IBD?". The evidence for this is much less than is present to even support the previously proposed mechanism whereby TMEM16A is down-regulated in colonic epithelium. However, it has been shown previously that Ca^{2+}-activated Cl^- secretion decreases in the first couple days of DSS-exposure even though physical symptoms such as loose stools with copious amounts of mucus do not manifest until about day 5 of a one week exposure [1]. Also, animals treated with DSS have disrupted mucus barriers that typically prevent interaction between the host and the microbiome [7]. It has been demonstrated that activation of TMEM16A is crucial for release of Muc5AC, however that study was conducted in human bronchial epithelial cells [8]. Muc5AC and similar proteins like it are necessary for maintaining the mucosal mucus barrier. Applying this knowledge, it is plausible that down-regulation of TMEM16A in DSS-colitis or potentially IBD could cause a decrease in Muc2 protein (more common in the intestine) secretion and overall disruption in the mucus barrier lining the colonic lumen. This would eventually lead to increased interaction between the microbiome and the host, which would elicit an inflammatory response. While this is highly speculative, it does provide a plausible route of further investigation.

KCNQ2/3 and the Enteric Nervous System

The ENS has a vast supply of neurons along the entire gastrointestinal tract. Previous research has demonstrated that the ENS can control local blood flow, motility of the tract, and influence electrolyte transport [9]. As far as ENS control over electrolyte transport, previous studies have demonstrated that application of TTX (Na_V inhibitor) or atropine (muscarinic antagonist) inhibits on-going Cl^- secretion via inhibition of I_{SC} [10, 11]. Our study was similar in setup, however, we focused on KCNQ channels and their contribution to resting membrane potential in enteric neurons. Activation of KCNQ channels with basolateral flupirtine was able to inhibit the observed I_{SC} in full thickness tissue from murine distal colon. This was achieved via inhibition of neurotransmitter release from enteric neurons that were substantially hyperpolarized. Application of TTX following flupirtine was practically unable to decrease the measured I_{SC}. Also, pre-incubation with flupirtine prior to stimulation with nicotine resulted in an unresponsiveness of the tissue. Application of flupirtine on the T_{84} colonic epithelial cell line further implicated that effect was mediated through the ENS, since the monolayers were unresponsive to the drug. However, flupirtine is a non-specific activator of KCNQ channels, therefore the use of immunofluorescence was employed to demonstrate the presence of KCNQ2 and KCNQ3 in enteric neurons.

The previously mentioned work seems to indicate that activation of KCNQ channels in enteric neurons can lead to inhibition of neurotransmitter release. Unfortunately, functional evidence of the exact channels that contribute to the

observed response is lacking. While the use of a specific activator of KCNQ2/3 was utilized in the study, channel activators are prone to selectivity issues. A specific inhibitor to the channel would be of clear benefit to the study and future research. However, the only available KCNQ inhibitors are linopiridine and XE-991, which are both global KCNQ inhibitors. This means that a specific channel can not be identified from inhibition with either of the drugs. Also, KCNQ1 has been characterized to reside on the basolateral membrane of colonic epithelium and inhibition causes decreased apical Cl^- secretion due to loss of a favorable electrochemical gradient [12, 13]. So, application of either of the inhibitors causes a decrease in I_{SC}, when one might expect an increase due to increased firing of enteric neurons. Hopefully in the future better pharmacological tools (inhibitors) can be developed that will allow for this functional characterization, or the development of a conditional knock-out model with an enteric neuron promoter.

The Enteric Nervous System And Inflammatory Bowel Disease

While seemingly disconnected, the two previously presented studies have a potential common thread of IBD. Research has primarily focused on the immune response that is present within the tissue, as well as, the changes in electrolyte transport across the epithelial layer. However, it has been shown that inflammation is able to elicit a hyper-excitability of enteric neurons [14, 15]. It would be of personal future interest to evaluate the effects of DSS administration on the ENS from the standpoint of electrolyte transport and epithelial integrity. I would be curious to see if oral administration of KCNQ activators is capable of

attenuating the deleterious effects of DSS-colitis and for that matter IBD as a whole. Also, utilization of animal models with dysfunctional enteric KCNQ channels with DSS administration would be interesting to characterize the severity of colitis as well as alterations in epithelial transport. Hopefully in the near future, activators truly specific to KCNQ2/3 will become available and allow for this evaluation.

References

1. Chassaing, B., et al., *Dextran sulfate sodium (DSS)-induced colitis in mice.* Curr Protoc Immunol, 2014. **104**: p. Unit 15 25.
2. Kanthesh, B.M., G.I. Sandle, and V.M. Rajendran, *Enhanced K(+) secretion in dextran sulfate-induced colitis reflects upregulation of large conductance apical K(+) channels (BK; Kcnma1).* Am J Physiol Cell Physiol, 2013. **305**(9): p. C972-80.
3. Hirota, C.L. and D.M. McKay, *Loss of Ca-mediated ion transport during colitis correlates with reduced ion transport responses to a Ca-activated K channel opener.* Br J Pharmacol, 2009. **156**(7): p. 1085-97.
4. Diaz-Granados, N., et al., *Dextran sulfate sodium-induced colonic histopathology, but not altered epithelial ion transport, is reduced by inhibition of phosphodiesterase activity.* Am J Pathol, 2000. **156**(6): p. 2169-77.
5. Zund, G., et al., *Interleukin-4 and interleukin-13 differentially regulate epithelial chloride secretion.* J Biol Chem, 1996. **271**(13): p. 7460-4.
6. Sun, H., et al., *Tgf-beta downregulation of distinct chloride channels in cystic fibrosis-affected epithelia.* PLoS One, 2014. **9**(9): p. e106842.
7. Petersson, J., et al., *Importance and regulation of the colonic mucus barrier in a mouse model of colitis.* Am J Physiol Gastrointest Liver Physiol, 2011. **300**(2): p. G327-33.

8. Huang, F., et al., *Calcium-activated chloride channel TMEM16A modulates mucin secretion and airway smooth muscle contraction.* Proc Natl Acad Sci U S A, 2012. **109**(40): p. 16354-9.

9. Furness, J.B., et al., *The enteric nervous system and gastrointestinal innervation: integrated local and central control.* Adv Exp Med Biol, 2014. **817**: p. 39-71.

10. Kuwahara, A., et al., *Effects of enteric neural stimulation on chloride transport in human left colon in vitro.* Dig Dis Sci, 1989. **34**(2): p. 206-13.

11. Biagi, B., Y.Z. Wang, and H.J. Cooke, *Effects of tetrodotoxin on chloride secretion in rabbit distal colon: tissue and cellular studies.* Am J Physiol, 1990. **258**(2 Pt 1): p. G223-30.

12. MacVinish, L.J., et al., *Xe991 reveals differences in K(+) channels regulating chloride secretion in murine airway and colonic epithelium.* Mol Pharmacol, 2001. **60**(4): p. 753-60.

13. Matos, J.E., et al., *Role of cholinergic-activated KCa1.1 (BK), KCa3.1 (SK4) and KV7.1 (KCNQ1) channels in mouse colonic Cl- secretion.* Acta Physiol (Oxf), 2007. **189**(3): p. 251-8.

14. Palmer, J., Wong-Riley Margaret, Sharkey Keith, *Functional alterations in jejunal myenteric neurons during inflammation in nematode-infected guinea pigs.* American Journal of Physiology, 1998. **275**(38): p. 922-935.

15. Linden, D.R., K.A. Sharkey, and G.M. Mawe, *Enhanced excitability of myenteric AH neurones in the inflamed guinea-pig distal colon.* J Physiol, 2003. **547**(Pt 2): p. 589-601.